

Sensor and Simulation Notes

Note 175

May 1973

PL/PA 16 DEC 96

Approximation to a Biconical Source Feed
on Linear EMP Simulators
by Using N Discrete Voltage Gaps

F. M. Tesche
Zoe Lynda Pine

The Dikewood Corporation

Abstract

This note studies the effect of approximating a biconical source feed on a linear EMP simulator by using N source gaps having uniform field distributions and being suitably located in the source region. One method for positioning the sources and determining their firing times is discussed, and numerical results for the radiated fields for various numbers of sources are presented and compared with the exact biconical results reported in SSN 110.

DI 91-1971

I. Introduction

One method used for producing pulsed electromagnetic fields for the purpose of studying the effects of nuclear EMP on systems is to employ a linear antenna with a pulsed driving source. As is well known, the high frequency behavior of such a simulator is dictated primarily by the structure of the antenna source region (and of course, upon the internal structure of the driving source), whereas the low-frequency behavior is mainly dependent on the total length of the simulator, as well as the presence of impedance loading along the structure. In the time domain, this implies that the early time response of the structure is dependent upon the source gap and the late time response is dependent on the loading and overall length.

As the nuclear EMP is a fast rising waveform with a slowly decaying exponential-like tail, it is desirable to construct the EMP simulator to produce fields having similar characteristics. The low frequency/late time behavior of such simulators has been studied by a number of investigators, and will not be discussed here. In this note, the early time characteristics of the simulator will be treated. As a result, it is possible to neglect the finite length of the simulator and consider the source gap to be located on an infinitely long, perfectly conducting cylinder of radius a .

In order to produce a fast rising radiated field, it has been shown⁽²⁾ that the biconical antenna is a suitable structure. In applying this to the linear EMP simulator, one method is to use the biconical geometry for the source region and connect it to a cylindrical antenna, as shown in Figure 1a. The driving source of V_0 volts may be positioned at the common apex of the two cones. One difficulty with this arrangement, however, is that there may be substantial arcing within the relatively small source region since the value of V_0 will be quite large in order to produce a large EMP.

One possible way to overcome this difficulty is to locate the driving sources on the extension of the cylindrical boundary over the biconical source region in such a manner that the radiated field is the same as that obtained from the biconical launcher.

In a previous note, Barnes⁽¹⁾ has computed the time dependent radiated fields from these equivalent sources on the surface of the cylinder as shown in Figure 1b. In actual practice, however, it is difficult to specify a continuous distribution of equivalent sources on the surface. For this reason, the structure treated by Barnes is difficult to realize physically.

As an approximation to the continuous distribution of equivalent sources, one could consider locating N cylindrical sources or bands having a constant electric field across them in such a way as to closely resemble the biconical field (Fig. 1c). As the number N increases, the radiated field will approach that computed for the biconical feed, but with much less possibility of air break-down as the impressed voltage V_0 is applied over a much larger region.

The problem of transient radiation from a single finite source gap or band with an assumed constant electric field has been discussed in a previous note.⁽⁸⁾ In this note, the results for the single band are combined to yield an approximation to the radiated field from the biconical source. The effect of varying the number of gaps, N , is studied and the results are compared to the case discussed by Barnes which is the limiting case as $N \rightarrow \infty$.

It should be pointed out that the results to be presented in this note may be applied to other types of EMP simulators, such as TORUS and other hybrid geometries as long as the local geometry in the source region is approximately straight.

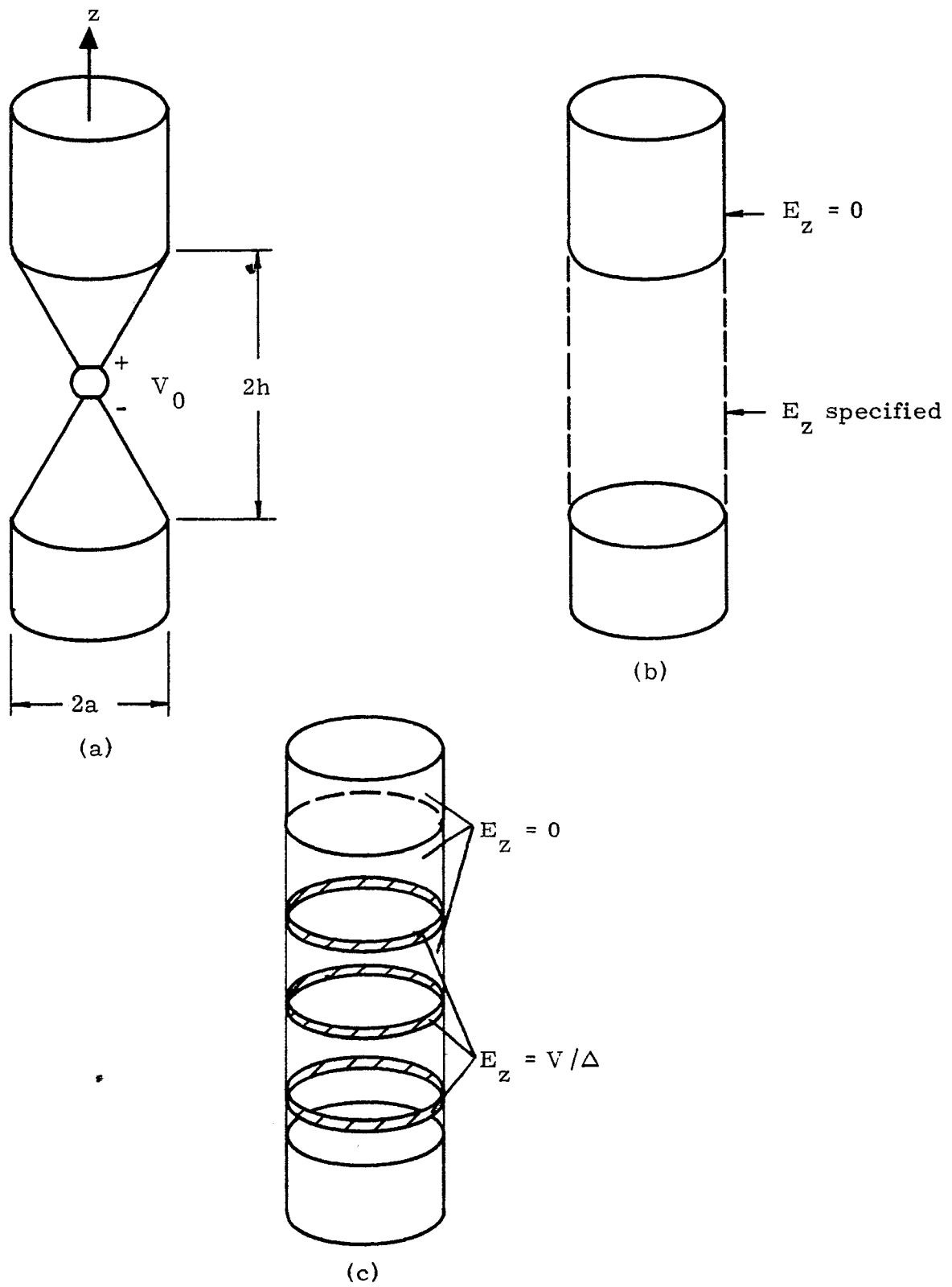


Figure 1. The biconical source and various approximations.

II. Formulation for the Single Finite Gap

The point of departure for the analysis of the antenna with N source bands approximating a biconical feed is to develop an expression for the field radiated from a single finite source gap as outlined in SSN 159.

Consider an infinite perfectly conducting cylinder of radius a and a finite source gap of width Δ centered at $z = 0$ as shown in Figure 2. At time $t = 0$ it is assumed that a voltage of V volts is impressed over the gap. It is then desired to compute the radiated field E_θ at some angle θ' .

The method to be employed in treating this problem involves using, as a Green's function, the time-domain radiated field for a slice generator exciting the antenna. By integrating this solution over the distribution of equivalent sources on the finite gap, the total solution can be determined.

In a paper by Papas,⁽⁷⁾ the far zone time-harmonic electric field, E_θ , produced by a delta-gap source on an infinite antenna is given as

$$E_\theta(r, \theta, \omega) = \frac{V(\omega)}{-j\pi} \frac{1}{\sin \theta H_0^{(2)}(ka \sin \theta)} \frac{e^{-jkr}}{r} \quad (1)$$

with an assumed time dependence of $e^{j\omega t}$. Here $V(\omega)$ represents the phasor voltage across the delta gap, $H_0^{(2)}$ is the Hankel function of the second kind, $k = \omega/c$, and r , a , and θ are the parameters defined in Figure 2.

To determine the time domain radiated field from the delta gap, it is first noted that for a step voltage of V_δ volts across the gap, the frequency domain excitation is $V(\omega) = V_\delta/j\omega$. Changing to the Laplace transform variable s , where $s = j\omega$, and noting that $H_0^{(2)}(-jz) = (2j/\pi)K_0(z)$, Eq. (1) becomes

$$E_\theta(r, \theta, s) = \frac{V_\delta e^{-sr/c}}{2sr \sin \theta K_0(sa \sin(\theta)/c)} \quad (2)$$

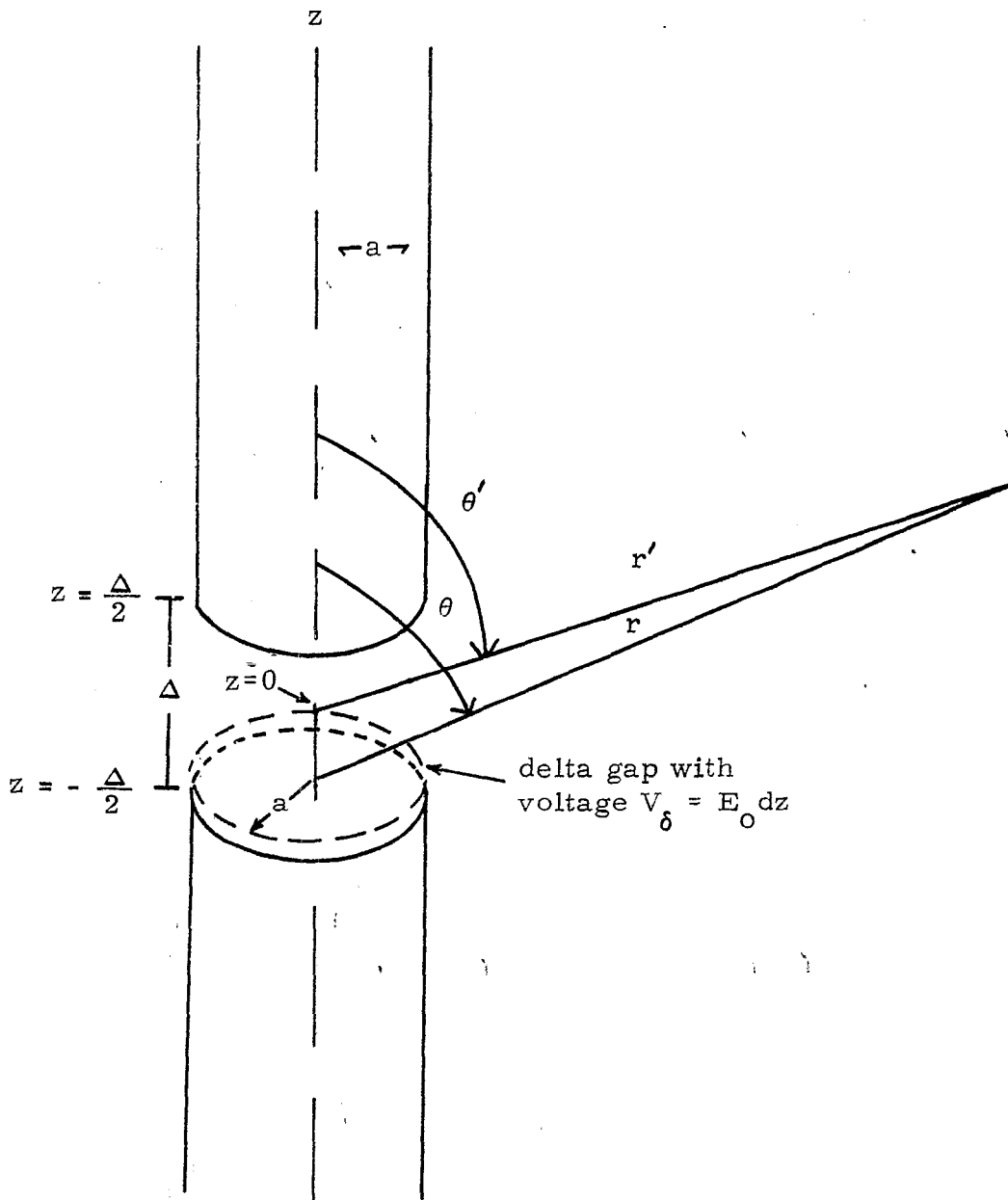


Figure 2. Infinite Antenna With a Finite Gap

Transforming Eq. (2) into the time domain by the inverse Laplace transform, one obtains

$$E_{\theta}(r, \theta, t) = \frac{V_{\delta}}{2r \sin \theta} \frac{1}{2\pi i} \int_{\sigma-j\infty}^{\sigma+j\infty} \frac{e^{s(t-r/c)}}{sK_0(sa \sin(\theta)/c)} ds \quad (3)$$

By closing the path of integration at infinity and taking into account the branch cut of the modified Bessel function K_0 along the negative real axis, Lee and Latham⁽⁴⁾ have shown that Eq. (3) can be expressed in terms of the integral

$$E_{\theta}(r, \theta, \tau) = \frac{V_{\delta}}{2r \sin \theta} \int_0^{\infty} \frac{e^{-\xi\tau/\sin\theta} I_0(\xi)}{K_0^2(\xi) + \pi^2 I_0^2(\xi)} \frac{d\xi}{\xi} \quad (4)$$

for $\tau \equiv (ct - r)/a > -\sin \theta$. In this expression, I_0 is a modified Bessel function. The evaluation of this integral thus provides the radiated electric field as a function of the normalized retarded time τ .

It should be pointed out in passing that Eq. (4) is not a strictly rigorous solution to the problem of radiation from a slice generator on the infinite cylinder. In obtaining the time domain response by the inverse Laplace transformation technique, it is necessary to know the spectrum of the electric field accurately for all frequencies. For any finite observation point r , it is always possible to find a low frequency ω_0 such that Eq. (1) is not valid since r is not in the far field. In the time domain, this implies that the very late time results of Eq. (4) will be in error. This effect is discussed by Latham and Lee.^(4,5)

To determine the transient radiated field from the finite gap of width Δ , it may be assumed that in the gap there are an infinite number of slice generators, each of voltage $V_{\delta}(z) = E_0(z)dz$. For convenience, it will be assumed that the electric field distribution over the finite source gap is a constant, given by $E_0 = V/\Delta$. Substituting this into Eq. (4) and integrating over the source gap gives the following equation for the time dependent radiated field

$$E_{\theta}(r', \theta', t) = \int_{-\Delta/2}^{\Delta/2} \frac{V dz}{2\Delta r \sin\theta} \int_0^{\infty} \frac{e^{-\xi(ct-r)/a \sin\theta} I_0(\xi)}{K_0^2(\xi) + \pi^2 I_0^2(\xi)} \frac{d\xi}{\xi} U\left(\frac{ct-r}{a} + \sin\theta\right) \quad (5)$$

where $U\left(\frac{ct-r}{a} + \sin\theta\right)$ is a unit step function introduced to account for the causality requirements inherent in Eq. (4). From Figure 1, it is seen that θ and r vary with the coordinate z . However, certain approximations can be made which are as follows:

1. $\theta \approx \theta'$
2. $r \sim r'$ (except for r in the exponential)
3. $r = \sqrt{r'^2 + z^2 - 2r'z \cos\theta} \approx r' - z \cos\theta'$ (for r in the exponential)

Utilizing these approximations in Eq. (5), the normalized radiated electric field becomes

$$\frac{r' E_{\theta}(r', \theta', t)}{V} = \frac{1}{2\Delta \sin\theta'} \int_{-\Delta/2}^{\Delta/2} dz \int_0^{\infty} \frac{e^{-\xi\left(\frac{ct-r'+z \cos\theta'}{a}\right) \csc\theta'} I_0(\xi)}{K_0^2(\xi) + \pi^2 I_0^2(\xi)} \frac{d\xi}{\xi} U\left(\frac{ct-r'+z \cos\theta'}{a} + \sin\theta'\right) \quad (6)$$

With the definition of the normalized retarded time $\tau = \frac{ct-r'}{a}$ and $p = \left(\tau + \frac{z \cos\theta'}{a}\right) \csc\theta'$, Eq. (6) becomes

$$\frac{r' E_{\theta}}{V} = \frac{1}{2\Delta \sin\theta'} \int_{-\Delta/2}^{\Delta/2} dz \int_0^{\infty} \frac{e^{-\xi p} I_0(\xi)}{K_0^2(\xi) + \pi^2 I_0^2(\xi)} \frac{d\xi}{\xi} U(p \sin\theta' + \sin\theta') \quad (7)$$

Defining the function $F(p)$ as

$$F(p) = \int_0^{\infty} \frac{e^{-\xi p} I_0(\xi)}{K_0^2(\xi) + \pi^2 I_0^2(\xi)} \frac{d\xi}{\xi} \quad (8)$$

Eq. (7) becomes

$$\frac{r' E_{\theta}}{V} = \frac{1}{2\Delta \sin \theta'} \int_{-\Delta/2}^{\Delta/2} F(p(z)) U((p(z) + 1) \sin \theta') dz \quad . \quad (9)$$

This equation defines the far field transient radiation from an infinite antenna with a finite source region, having a uniform field distribution.

As mentioned in SSN 159, it is possible to derive asymptotic forms for both the early and late time behavior of the radiated field. These will not be repeated here.

III. Approximation of the Biconical Source Field by N Discrete Sources

Consider the biconical source region on the antenna as shown in Figure 3, where the parameters θ_b , θ_o , a , h and V_o are defined. As discussed by Baum,⁽²⁾ the time dependent electric field radiated from a biconical antenna has the expression

$$\vec{E}_b(r_o, t^*) = \frac{V_o(t^*) f_o}{r_o \sin \theta_b} \hat{\theta} \quad \text{for } \theta_b < \theta < \pi - \theta_b \quad (10)$$

with the retarded time $t^* = t - r_o/c$ and $f_o = \left\{ 2 \ln [\cot(\theta_b/2)] \right\}^{-1}$.

The tangential component of the electric field as evaluated on the extension of the cylindrical surface between $z = h$ and $z = -h$ is then given as

$$E_z = - E_b \sin \theta_o \hat{z}. \quad (11)$$

Noting that r_o will be \hat{z} on the surface of the antenna, Eq. (10) becomes

$$E_z = - \frac{V_o f_o \hat{z}}{\sqrt{z^2 + a^2}} U \left(t - \frac{1}{c} \sqrt{z^2 + a^2} \right) \quad (12)$$

for a step driving voltage $V_o(t) = V_o U(t)$.

The next step is to approximate the electric field in Eq. (12) by a series of N finite source gaps, each of voltage $V = V_o/N$ as shown in Fig. 1b. In SSN 84, Baum describes one possible method for positioning the N sources on the cylindrical surface over the gap, by dividing the surface into a number of equipotential bands. For the N sources, he defines $M = 2N$ bands over the source gap. This requires $2N + 1$ individual z coordinates and following SSN 84, they are given by

$$z_n = a \sinh \left[\frac{n}{N} \sinh^{-1}(h/a) \right] \quad n = -N, \dots, 0, \dots, N \quad (13)$$

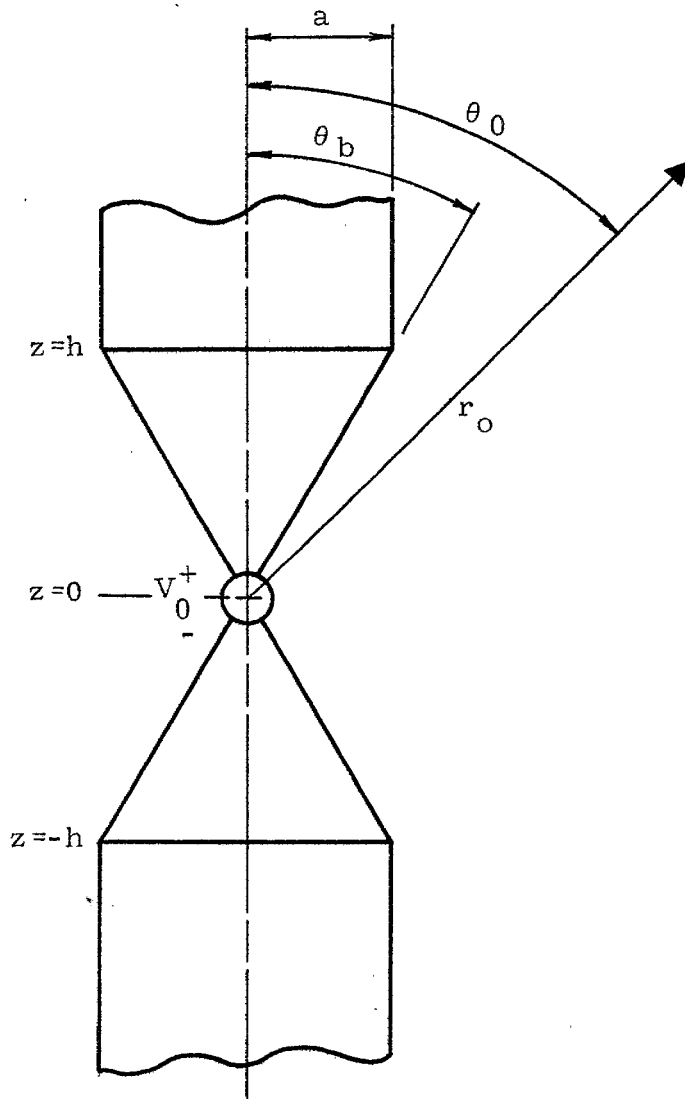


Figure 3. The biconical source region.

This relation defines the division points within the source region. Notice that the difference between the points increases near the ends of the region at $z = \pm h$, and also that the values of $z_{\pm N} = \pm h$ and $z_0 = 0$ are always fixed.

The positioning of the N sources depends upon whether N is even or odd. If N is odd, the sources, all having the same voltage V and width Δ are centered around z_n for $n = 0, \pm 2, \pm 4, \dots, \pm(N-1)$. For N even, all of the identical sources are centered around z_n for $N = \pm 1, \pm 3, \dots, \pm N-1$. In both of these cases, it is noted that the maximum size of Δ that can be employed is equal to $2z_1$, or z_2 depending on whether N is even or odd. Figures 4a and b show the positioning of these sources.

From Eq. (12) it is noted that the tangential electric field over the source region does not turn on everywhere at the same time. If the source of the biconical generator turns on at $t = 0$, it will be assumed that the N source gaps turn on at a time such that the uniform field within the gap is first non-zero at a time

$$t_n = \sqrt{z_n^2 + a^2} / c. \quad (14)$$

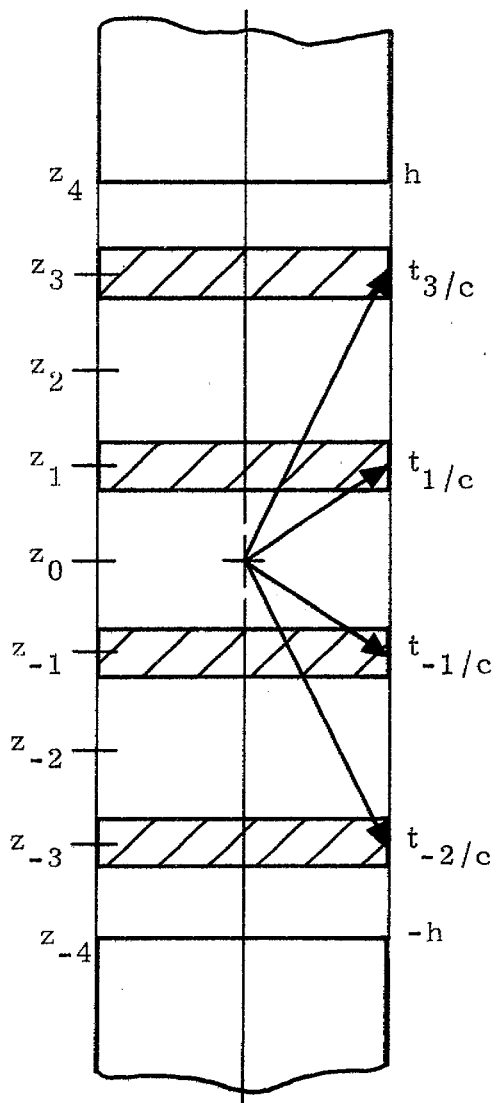
This equivalent source turn-on time is indicated graphically in Figures 4a and b.

To find the radiated field from the total collection of gaps, it is then necessary to sum the individual contributions, taking into account the differences in turn-on times of each source, and the differences of transit times from the sources to the observer. From Eq. (9), it is seen that the contribution from any particular source, as observed at an angle θ_o , first occurs for t such that

$$\left(t - \frac{r}{c}\right) + \frac{\Delta}{2c} \cos \theta_o + a \sin \theta_o = 0, \quad (15)$$

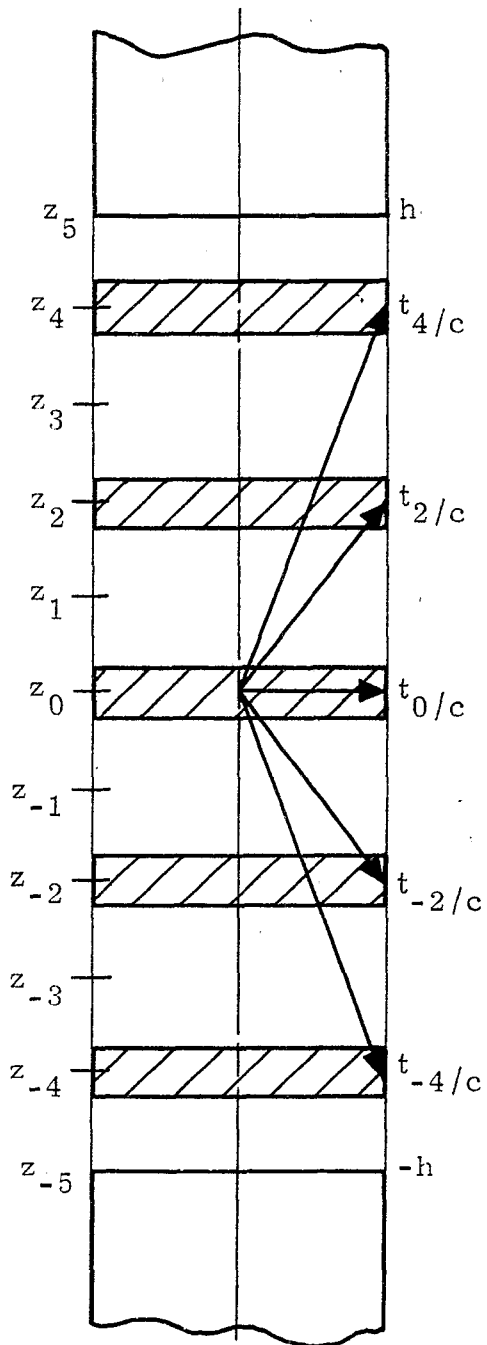
where r is the distance from the center of the gap in question, and the gap field turns on at $t = 0$. The observation angle θ_o in this note should not be confused with the bicone angle in SSN 110. The bicone angle here is referred to by θ_b .

For the observation being made at θ_o , as shown in Figure 5, it is noted that the distance r_n from the center of the n th gap may be referenced



Four driving sources of voltage $V = V_0/4$ and having a width Δ

Figure 4a. Position and turn-on times for far sources.



Five driving sources of voltage $V = V_0/5$ and having width Δ

Figure 4b. Position and turn-on times for five sources.

to r_0 by

$$r_n = r_0 - z_n \cos \theta_0 \quad (16)$$

where z_n is the location of the center of the gap. Considering the n th source gap and accounting for the turn on time t_n , Eq. (15) yields

$$\left(t - \frac{r_0}{c}\right) - t_n + \frac{z_n}{c} \cos \theta_0 + \frac{\Delta}{2c} \cos \theta_0 + \frac{a}{c} \sin \theta_0 > 0 \quad (17)$$

for the relation defining the time t at which the first effect of the n th source is observed in the far field. Using the definition of the retarded time $t^* = t - r_0/c$, the normalized time $T = ct^*/a$, and the definition of t_n in Eq. (14), the normalized turn-on time for the n th source is

$$T_n = \sqrt{1 + \left(\frac{z_n}{a}\right)^2} - \left(z_n + \frac{\Delta}{2}\right) \frac{\cos \theta_0}{a} - \sin \theta_0 \quad (18)$$

The total radiated field may then be obtained by summing all of the contributions from the gaps as determined by Eq. (9), and this result is expressed as

$$\frac{r_0 E_\theta(\theta_0, T)}{V_0} \sum_{\substack{n=-(N-1) \\ \text{odd } n \text{ or} \\ \text{even } n}}^{n=(N-1)} \frac{r_0 E_\theta(\theta_0, T - T_n)}{V} U(T - T_n)$$

where it is assumed that the time dependence of E_θ in Eq. (9) is expressed in terms of $T = ct^*/a$, and $V = V_0/N$.

In the application of this formula, it is necessary to specify the source gap size Δ . One possible way, which shall be employed in the numerical study presented in Section IV, is to use the maximum Δ which can be put into the source region without having an overlap. This is given by $\Delta = 2z_1$, for N odd and $\Delta = z_2$ for N even.

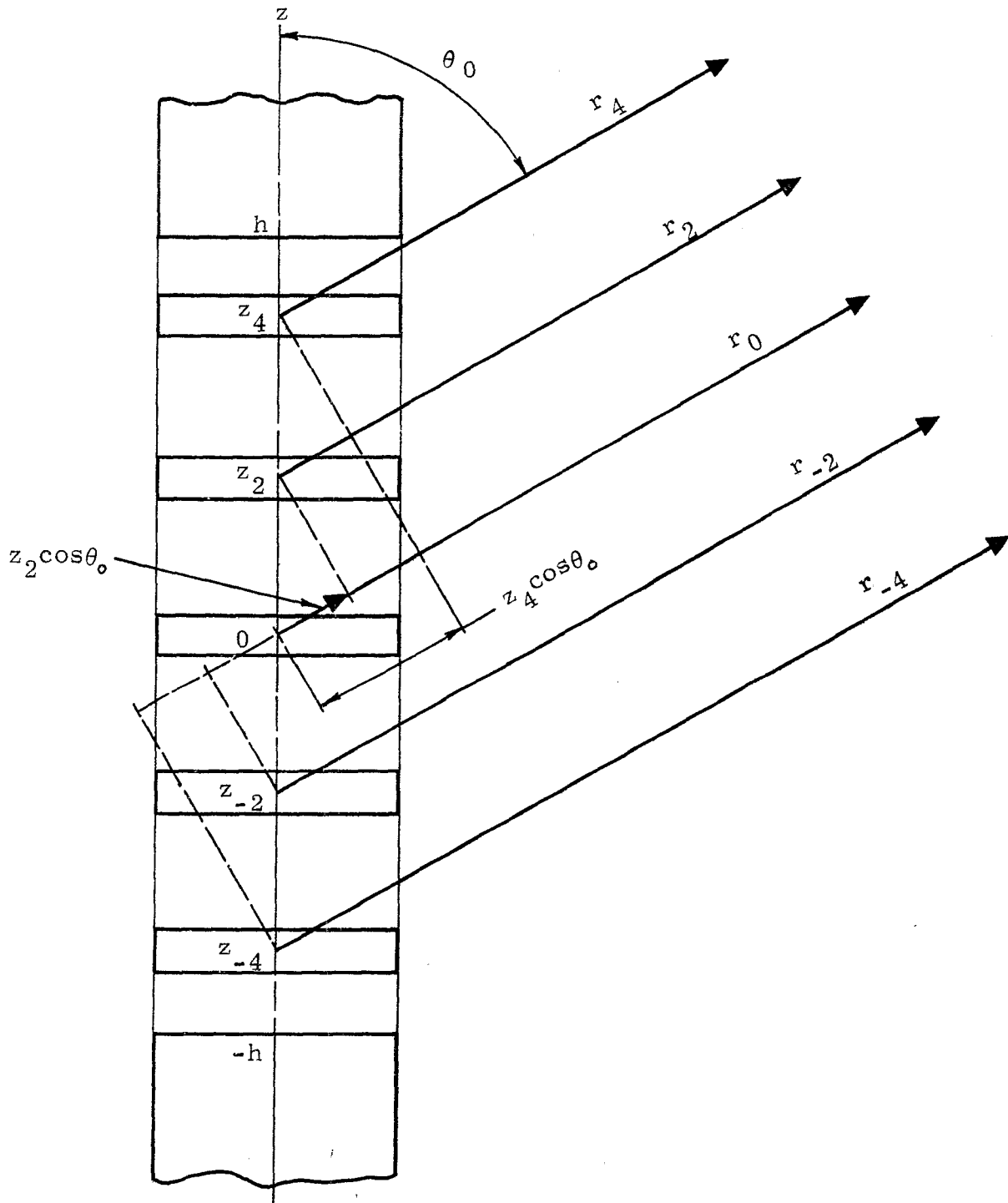


Figure 5. Differences in distance from the various sources to the far field observation point.

IV. Numerical Results

Using the procedure outlined in Section III, the radiated field from a finite number of discrete sources chosen so as to approximate the time dependent field radiated from a biconical source was calculated for various numbers of sources. Figures 6 through 29 show these fields for bicone angles $\theta_b = \tan^{-1}(a/h) = .8, .6, .4, \text{ and } .2 \pi/2$ and for observation angles $\theta_o = 1.0, .8, .6, .4, .2, \text{ and } .05 \pi/2$. For each case, there have been 1, 2, 3, 4, 5, 8, 10 and 15 sources considered. Note that these radiated fields are presented as a function of normalized retarded time $T = ct^*/a = c(t - r_o/c)/a$.

In addition to the fields produced by the discrete sources, Figures 6 through 29 show the radiated field from the biconical source as computed in Ref. (1). It is seen that as the number of source gaps increases, the curves from the discrete array tend to converge to those for the bicone source.

For observation angles $\theta_o = \pi/2$, it is seen that the contribution from each of the N sources results in an infinite response in the far field when the effect of the source is first felt at the observation point. This effect is discussed in Ref. (8).

It should be remembered that the source gap size Δ has been chosen to be the largest possible for the number N, as described in the previous section.

These curves are briefly summarized in Figures 30 through 33 where the maximum overshoot, δ , between the two curves is plotted for various values of θ_o and θ_b as a function of the number of sources. Note that these curves are plotted as continuous functions, but they are really defined only for integer values of N. The cases for $\theta_o = \pi/2$ have not been plotted, as the spikes in those curves are infinite, thereby yielding an infinite value of δ .

Final summary curves are presented in Figures 34 through 37 where the normalized turn-on times of waveforms radiated by the discrete array of sources is plotted. This turn-on time, denoted by T_o , is defined as the normalized time at which the first effect of any source on the antenna first reaches the observer. Note that this comparison is done for only the illuminated region of the source, defined by $\theta_o \geq \theta_b$. This implies that the bicone field turns on at $T = 0$. As in the previous curves, these times are defined only at integer values of N , the number of sources, but have been portrayed as continuous functions for convenience. In general, the turn on time of the discrete source field is a negative quantity compared with the bicone field turn on time.

As seen from the curves of the radiated field, the case of $\theta_o = \pi/2$ is quite different from the other cases. The turn-on time for these is positive in general, for N even, and for odd values of N , the turn-on time happens to be at $T = 0$. As a result, the curve for this particular observation angle is dashed on the summary curves.

Key for Figures 6 through 29

		θ_o (in units of $\pi/2$) →					
		1.0	.8	.6	.4	.2	.05
θ_b (in units of $\pi/2$) ↓	.2	Fig. 6	7	8	9	10	11
	.4	12	13	14	15	16	17
	.6	18	19	20	21	22	23
	.8	24	25	26	27	28	29

Figures 6 through 29 present the time dependent radiated field from the biconical source, as observed at various observation angles θ_o and for various biconical angles θ_b . The above chart shows at a glance where the data is presented within these curves.

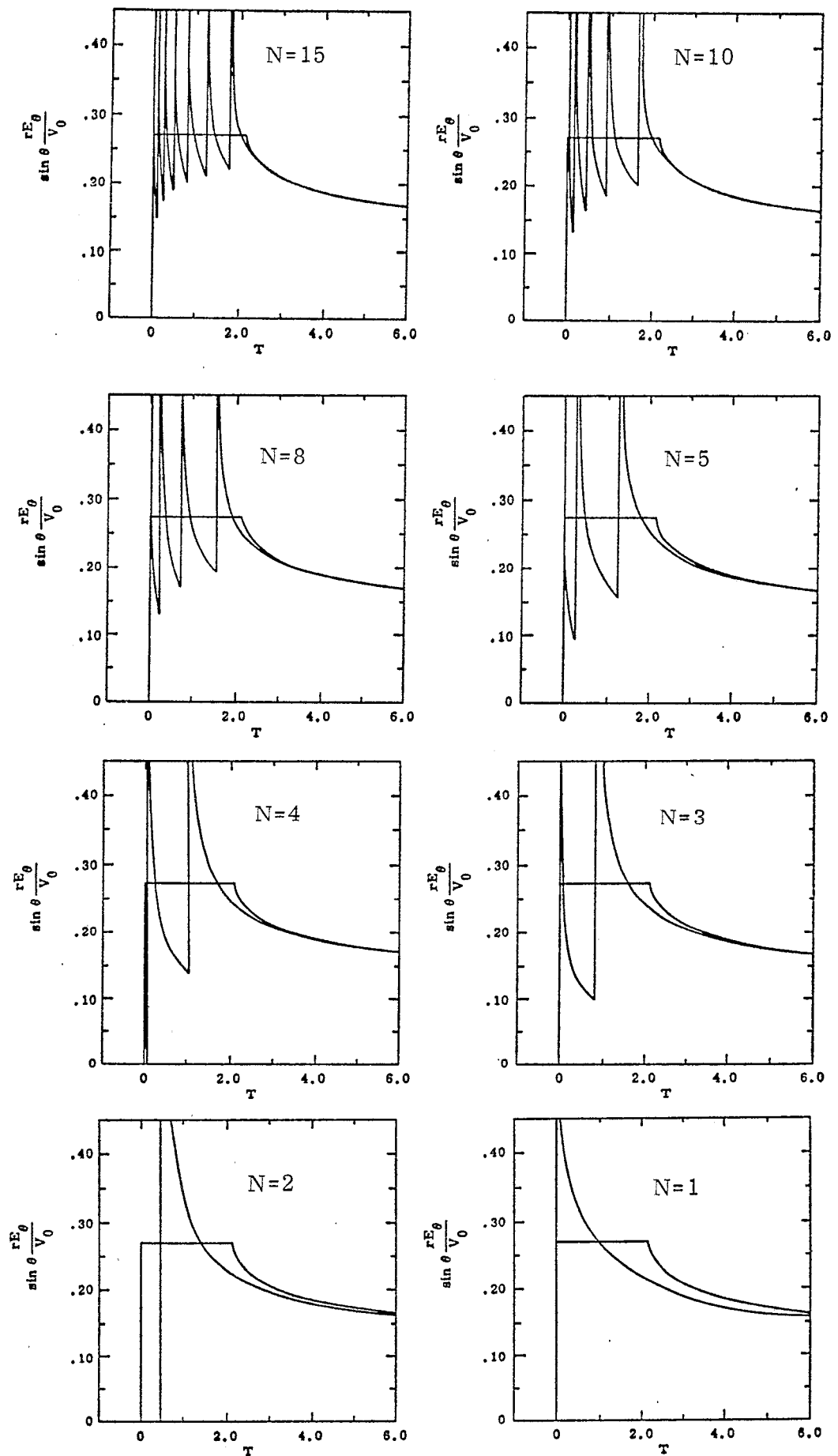


Figure 6. Radiation Field for bicone angle of $\theta_b = .2 \pi/2$ observed at $\theta_0 = 1.0 \pi/2$ for various values of source gaps, N .

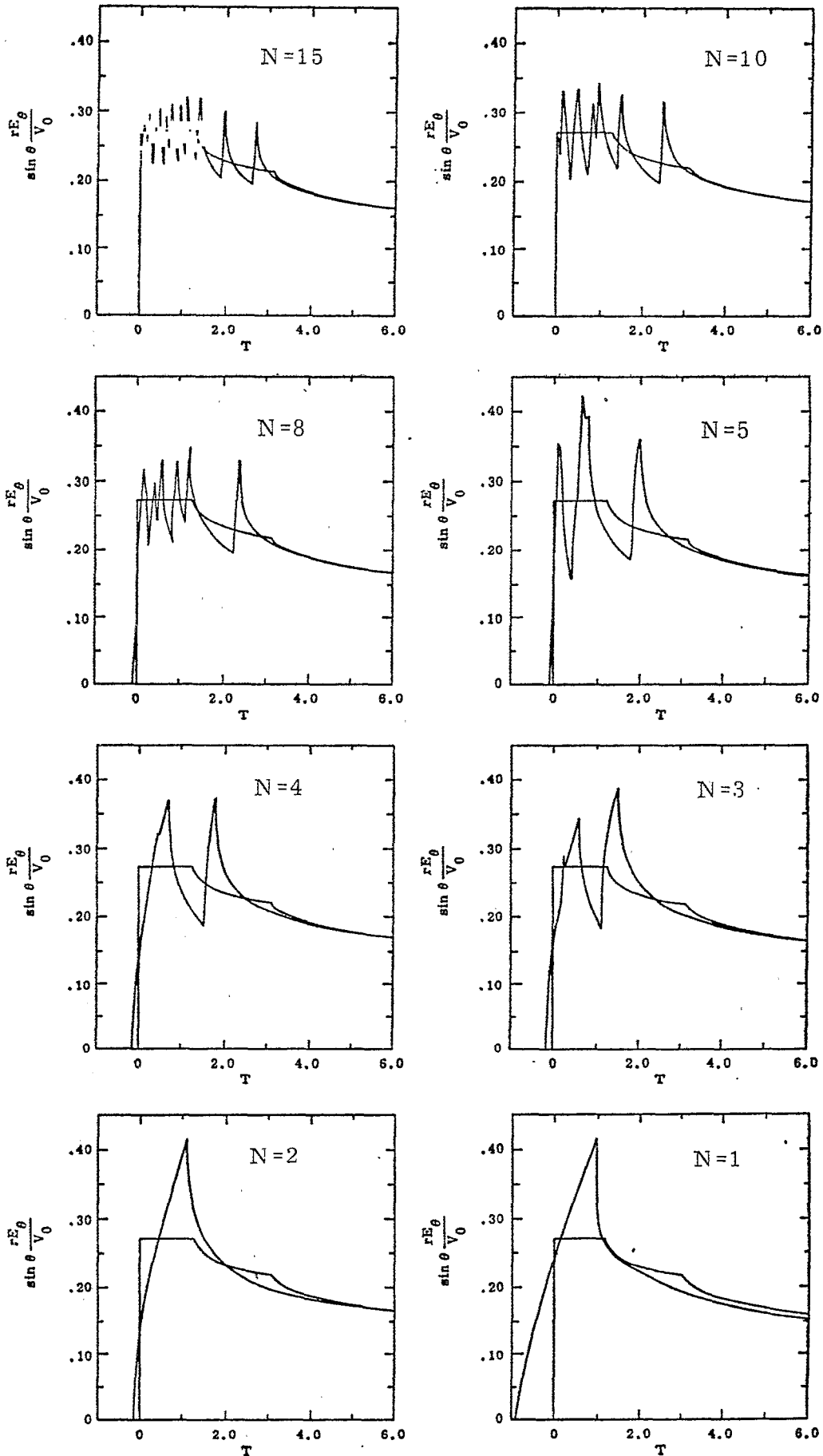


Figure 7. Radiation Field for bicone angle of $\theta_b = .2 \pi/2$ observed at $\theta_o = .8 \pi/2$ for various values of source gaps, N .

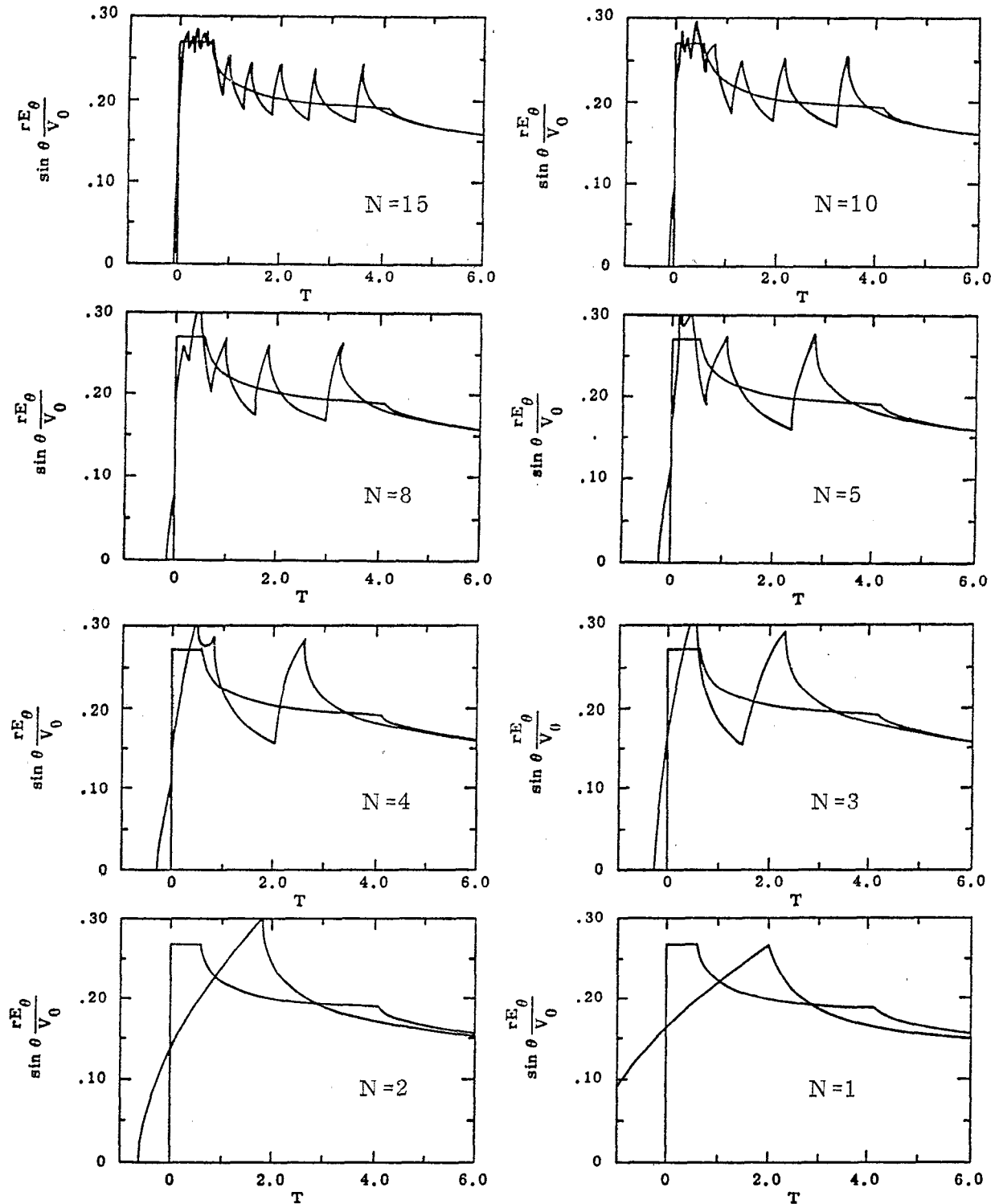


Figure 8. Radiation Field for bicone angle of $\theta_b = .2 \pi/2$ observed at $\theta_o = .6 \pi/2$ for various values of source gaps, N .

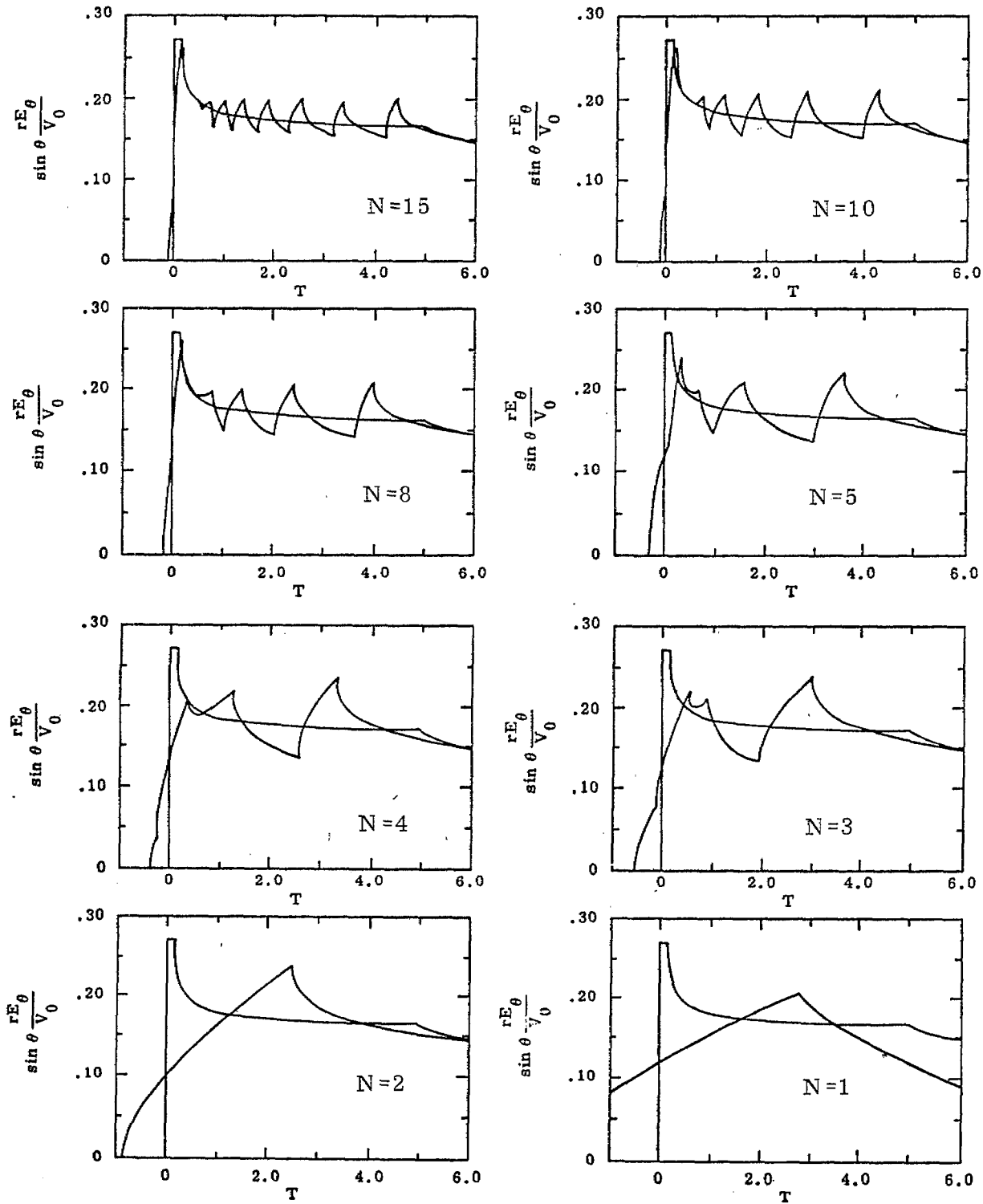


Figure 9. Radiation Field for bicone angle of $\theta_b = .2 \pi/2$ observed at $\theta_o = .4 \pi/2$ for various values of source gaps, N .

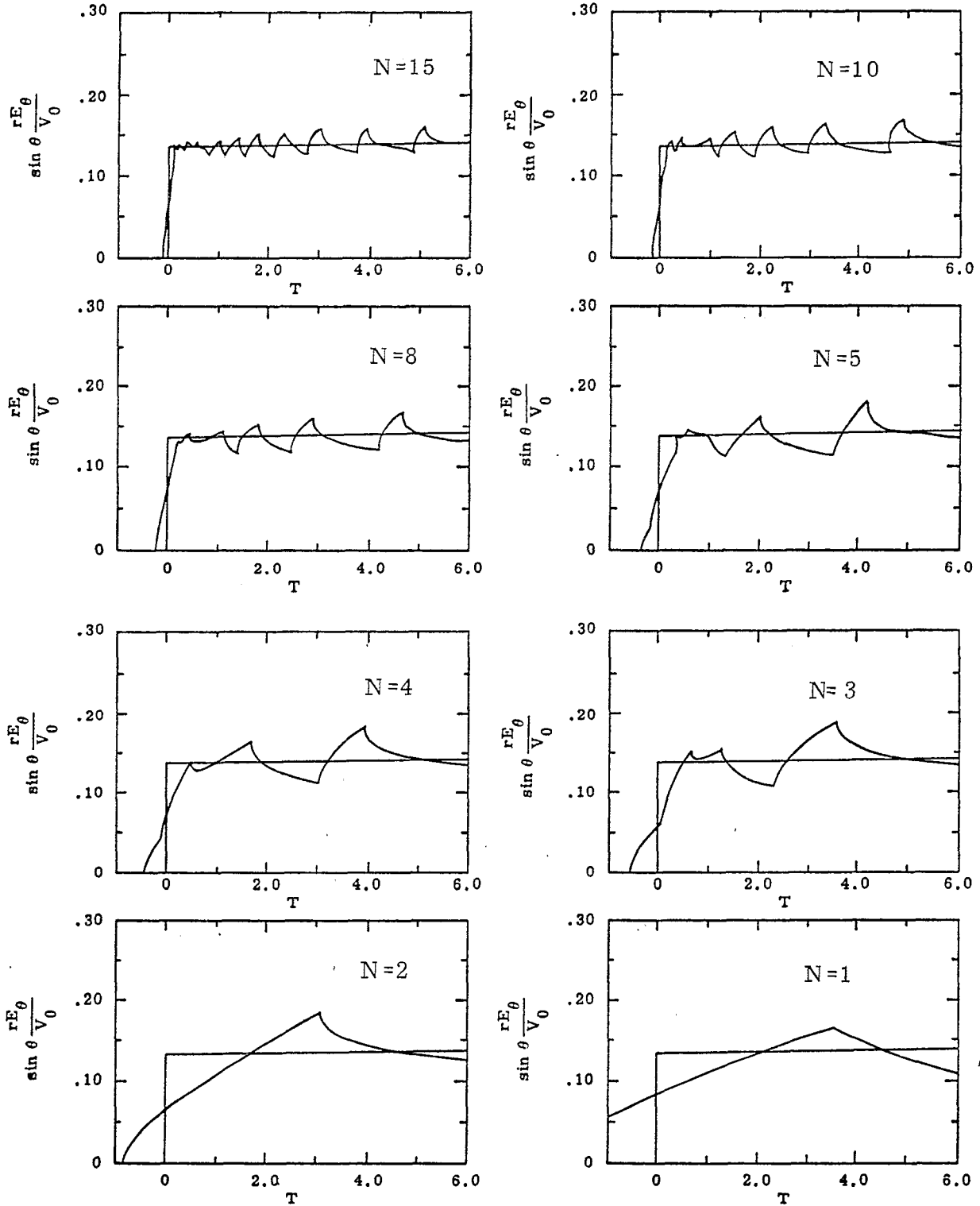


Figure 10. Radiation Field for bicone angle of $\theta_b = .2 \pi/2$ observed at $\theta_o = .2 \pi/2$ for various values of source gaps, N .

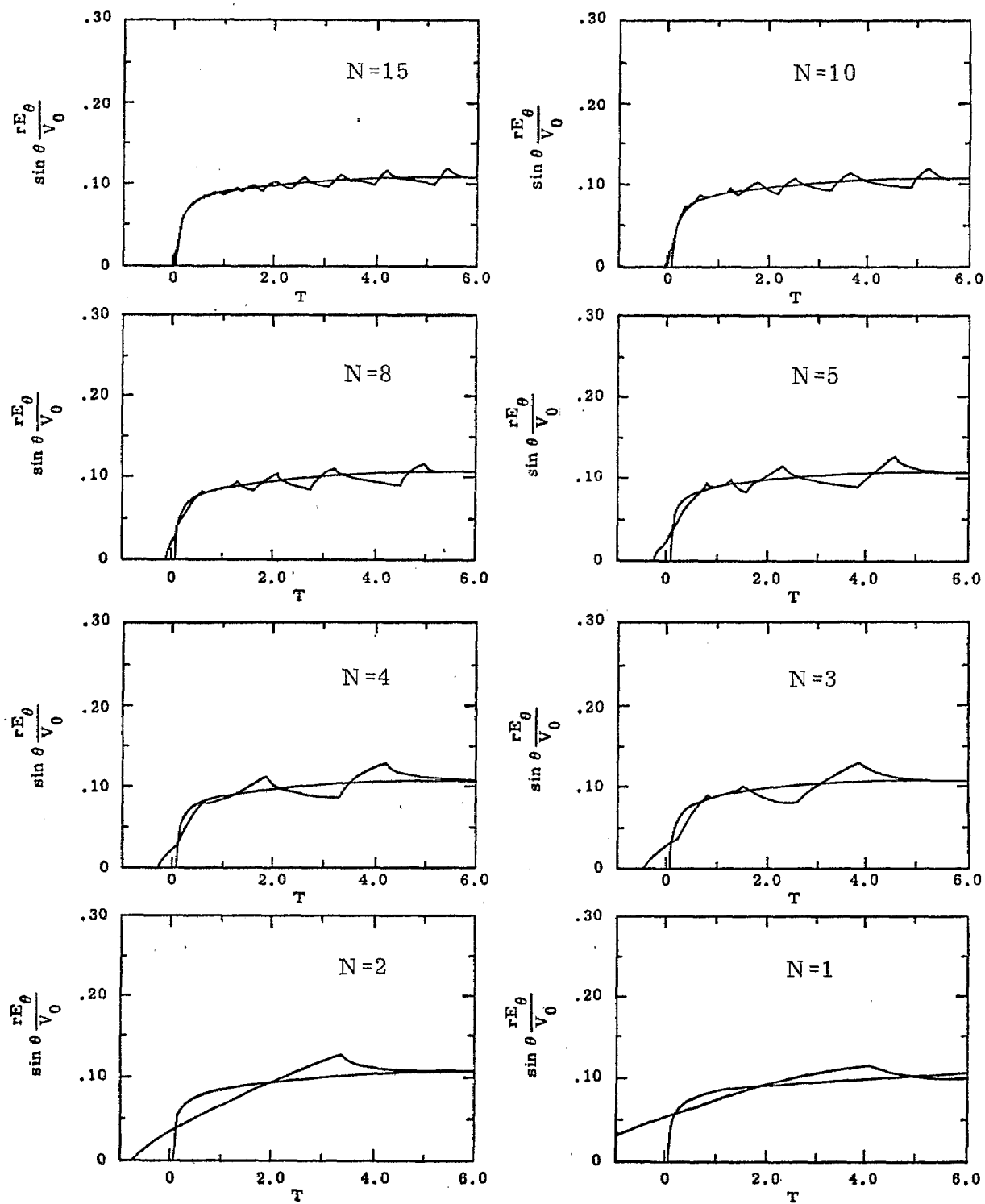


Figure 11. Radiation Field for bicone angle of $\theta_b = .2 \pi/2$ observed at $\theta_o = .05 \pi/2$ for various values of source gaps, N .

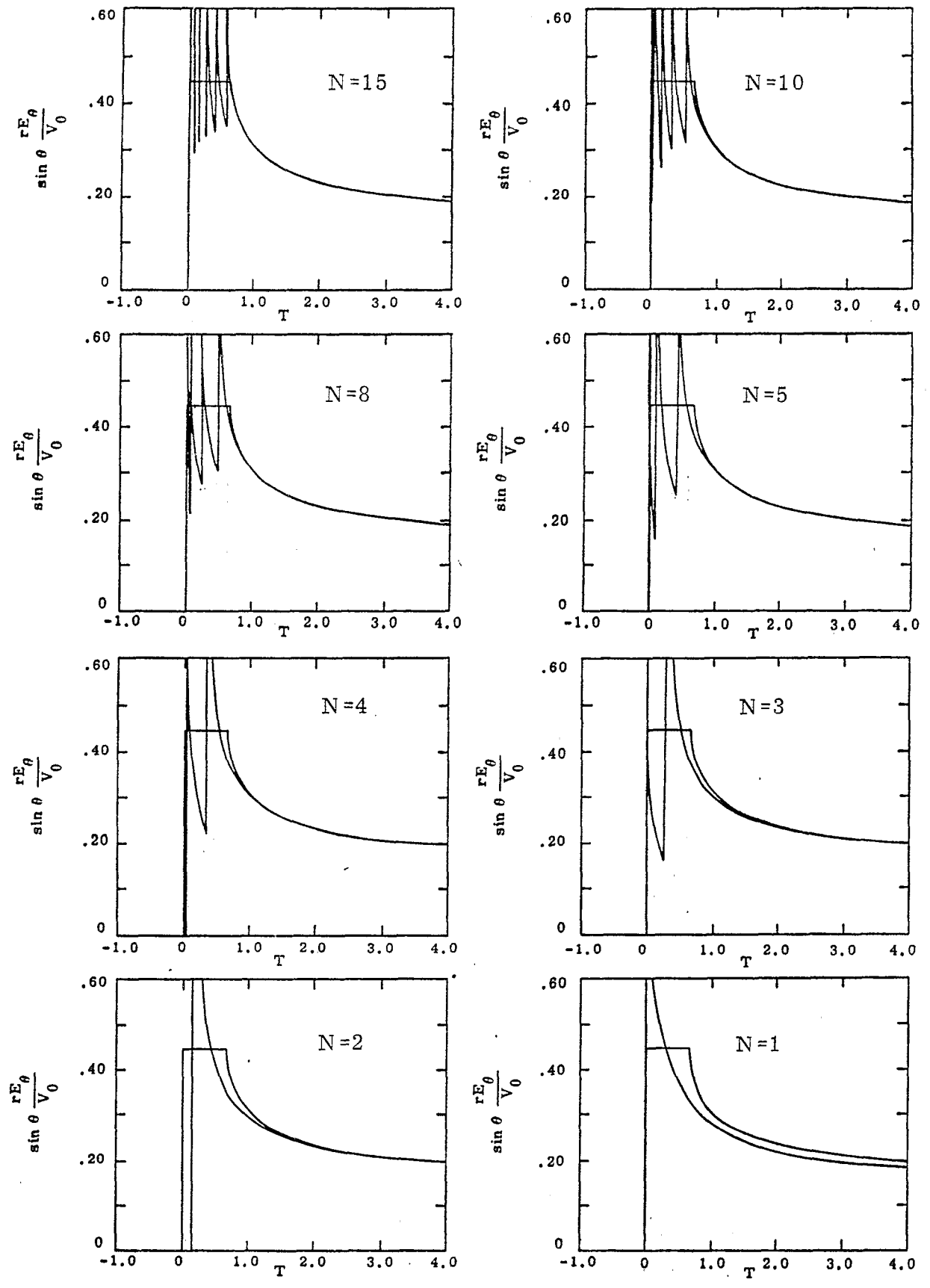


Figure 12. Radiation Field for bicone angle of $\theta_b = .4 \pi/2$ observed at $\theta_o = 1 \pi/2$ for various values of source gaps, N .

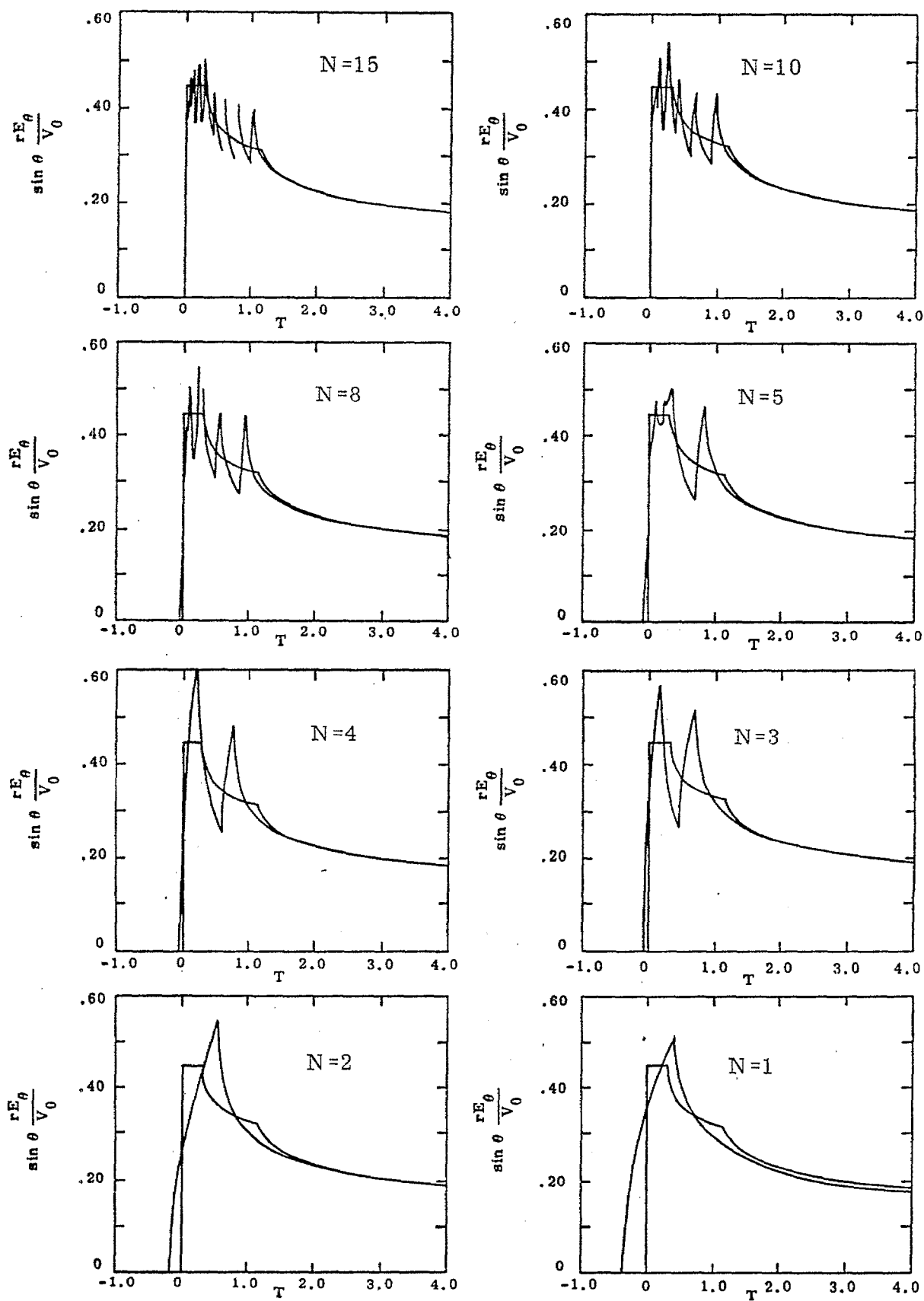


Figure 13. Radiation Field for bicone angle of $\theta_b = .4 \pi/2$ observed at $\theta_o = .8 \pi/2$ for various values of source gaps, N .

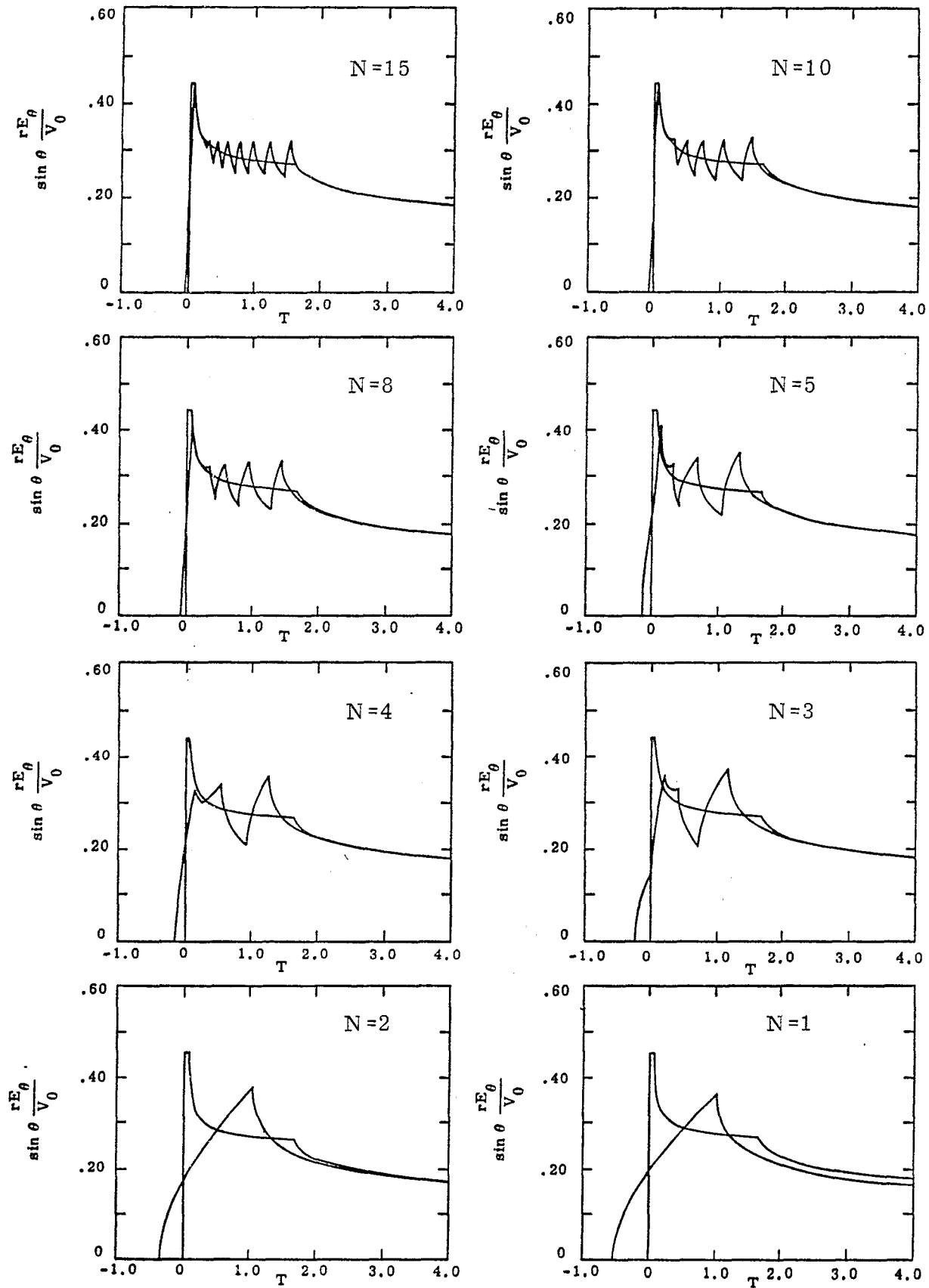


Figure 14. Radiation Field for bicone angle of $\theta_b = .4 \pi/2$ observed at $\theta_o = .6 \pi/2$ for various values of source gaps, N .

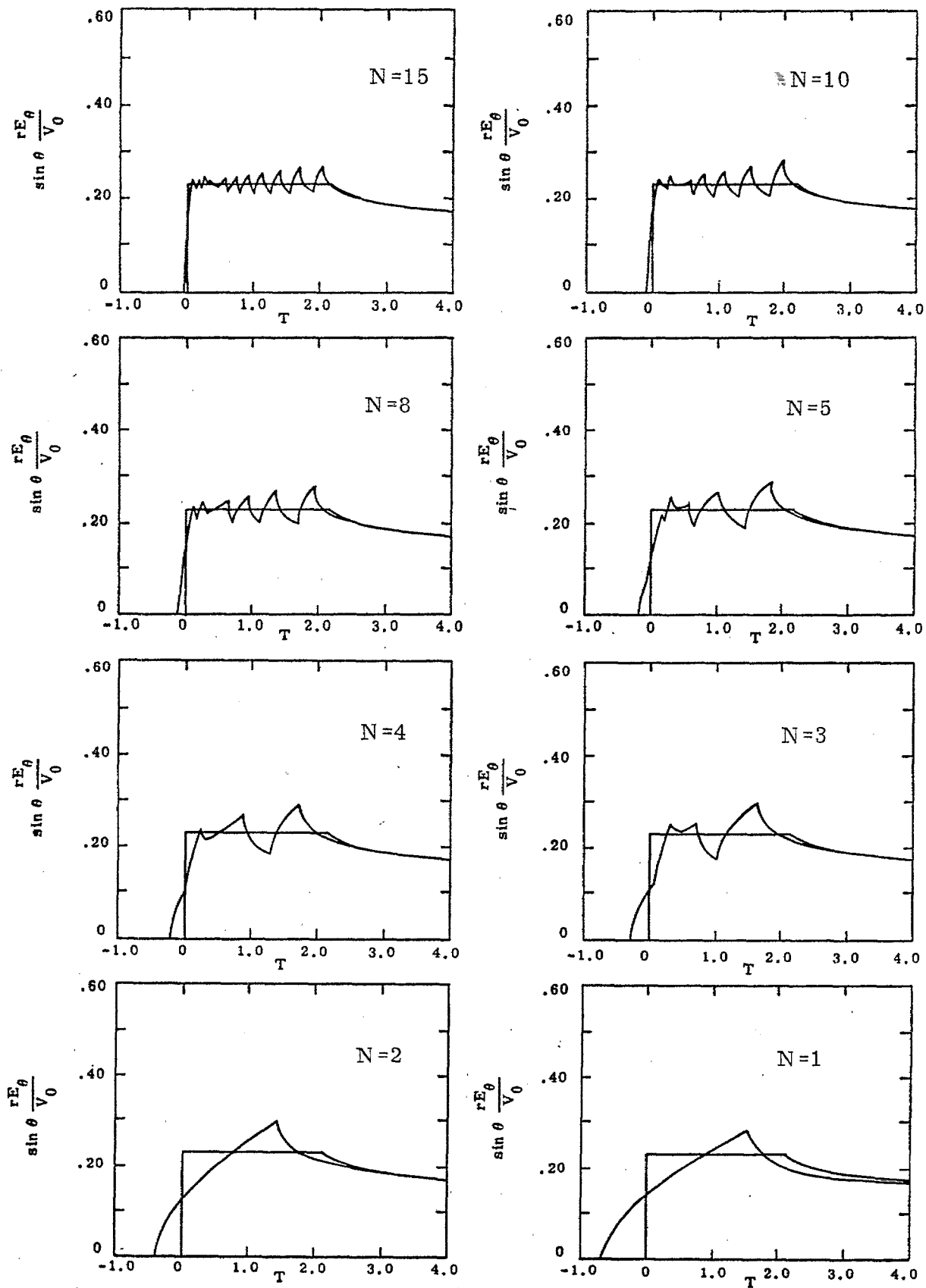


Figure 15. Radiation Field for bicone angle of $\theta_b = .4 \pi/2$ observed at $\theta_o = .4 \pi/2$ for various values of source gaps, N .

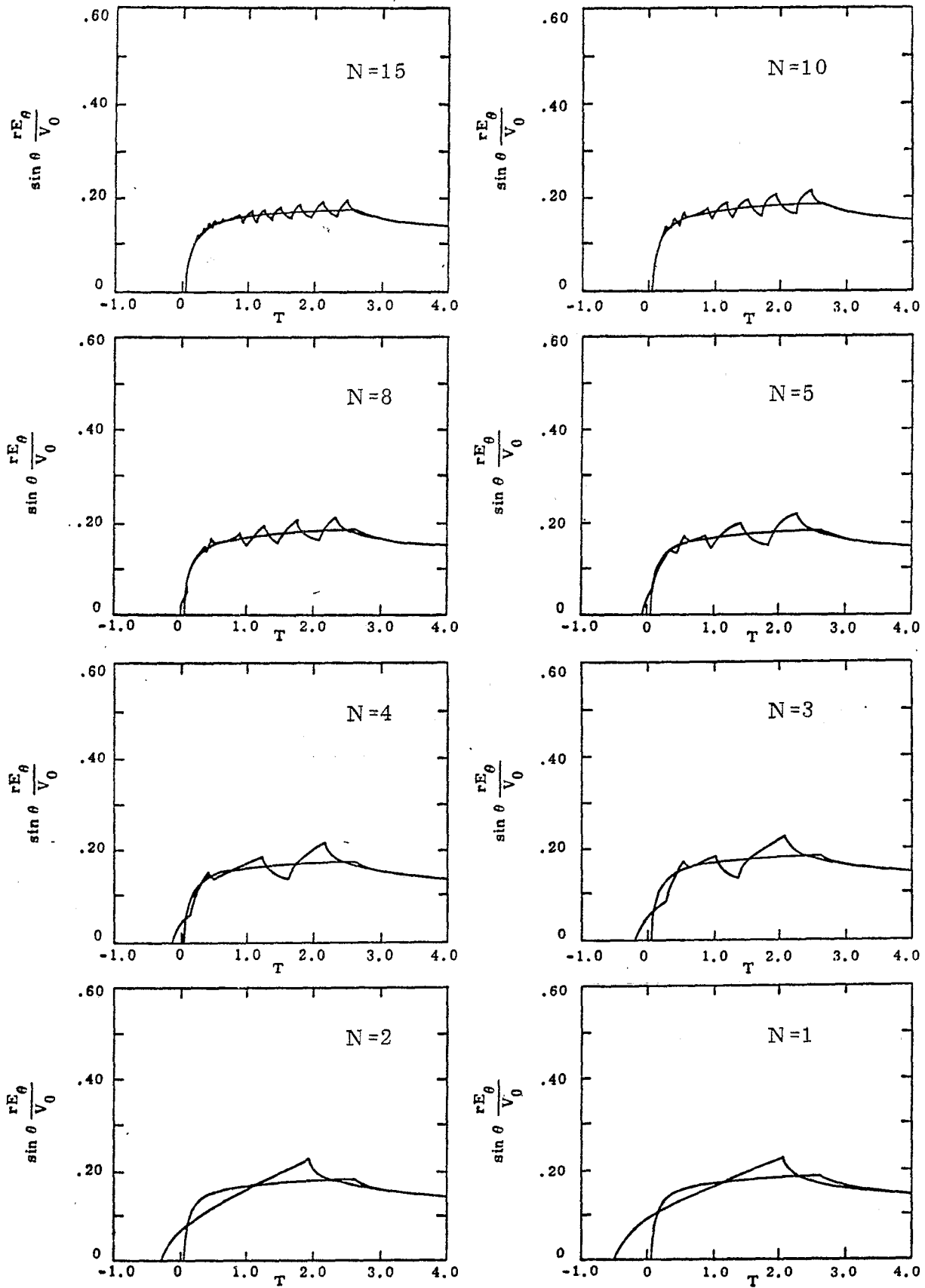


Figure 16. Radiation Field for bicone angle of $\theta_b = .4 \pi/2$ observed at $\theta_o = .2 \pi/2$ for various values of source gaps, N .

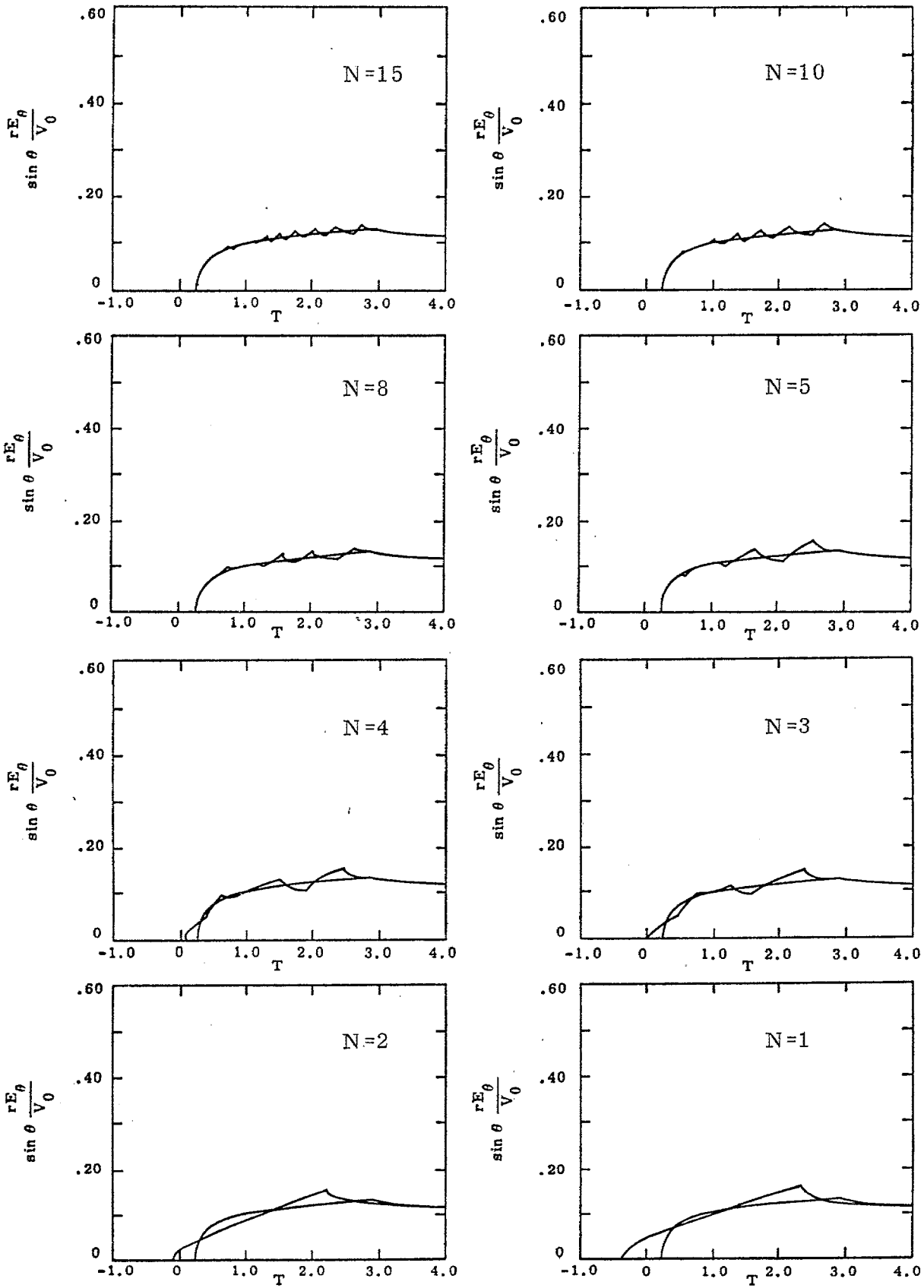


Figure 17. Radiation Field for bicone angle of $\theta_b = .4 \pi/2$ observed at $\theta_o = .05 \pi/2$ for various values of source gaps, N .

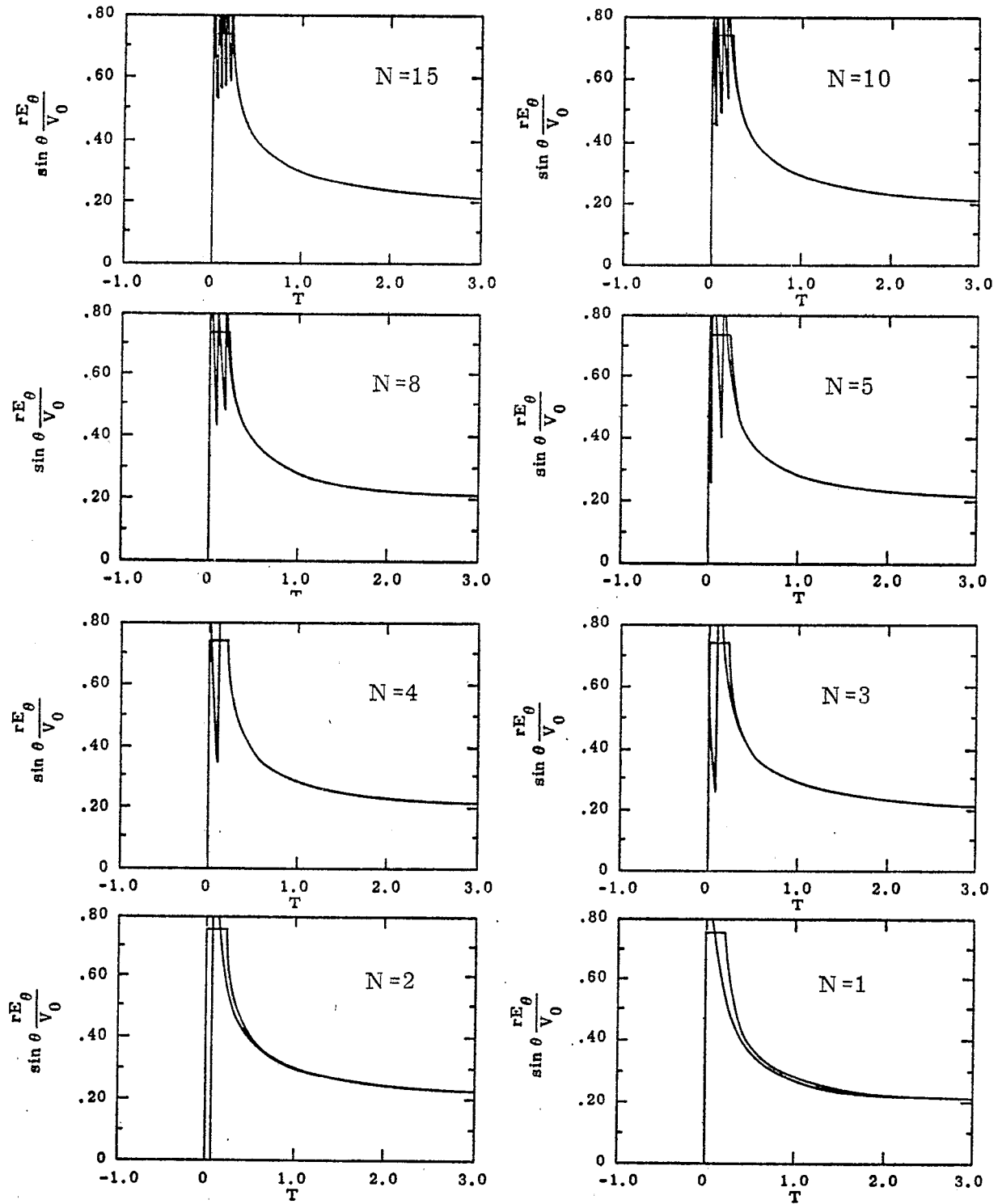


Figure 18. Radiation Field for bicone angle of $\theta_b = .6 \pi/2$ observed at $\theta_o = 1.0 \pi/2$ for various values of source gaps, N .

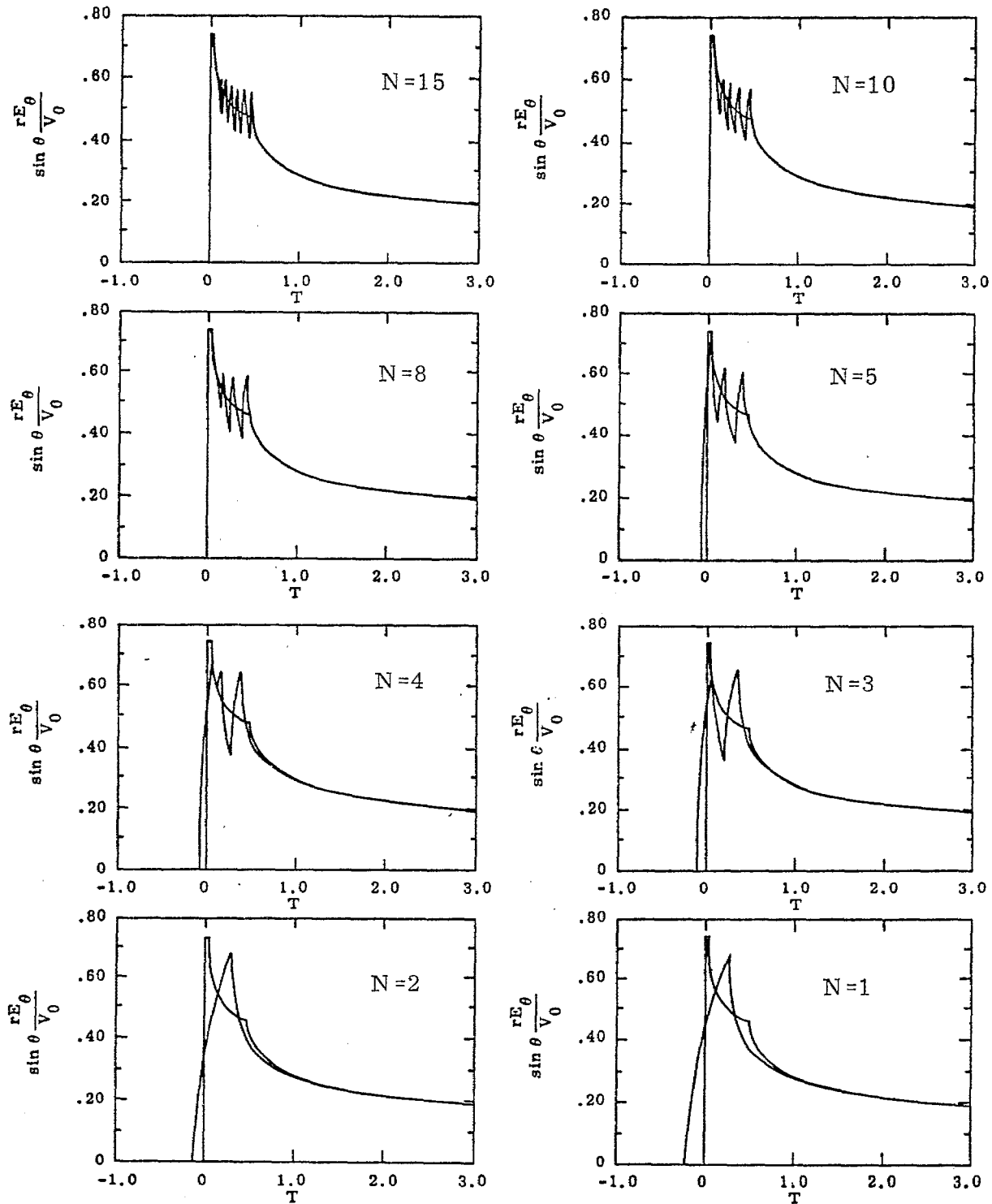


Figure 19. Radiation Field for bicone angle of $\theta_b = .6 \pi/2$ observed at $\theta_o = .8 \pi/2$ for various values of source gaps, N .

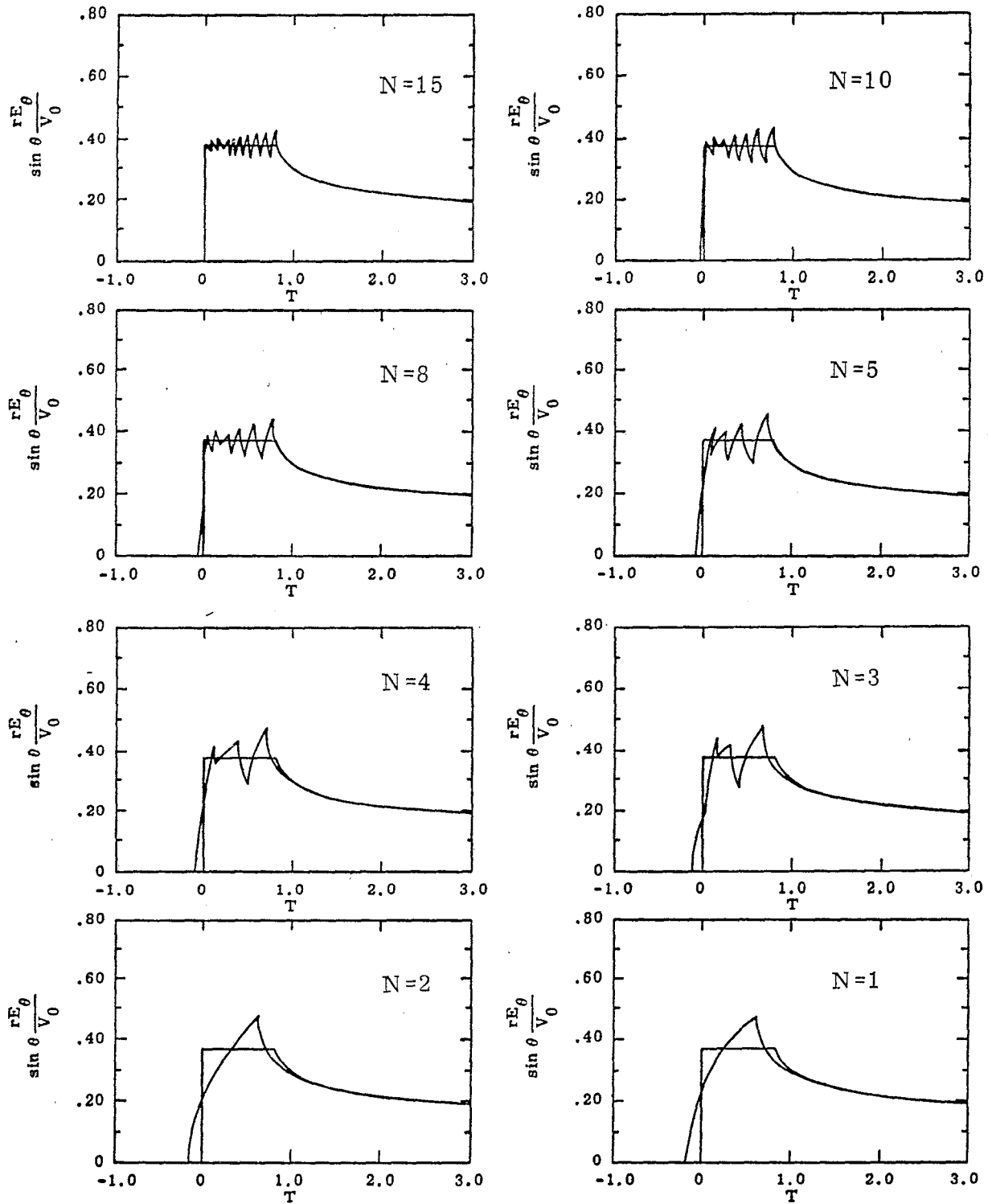


Figure 20. Radiation Field for bicone angle of $\theta_b = .6 \pi/2$ observed at $\theta_o = .6 \pi/2$ for various values of source gaps, N .

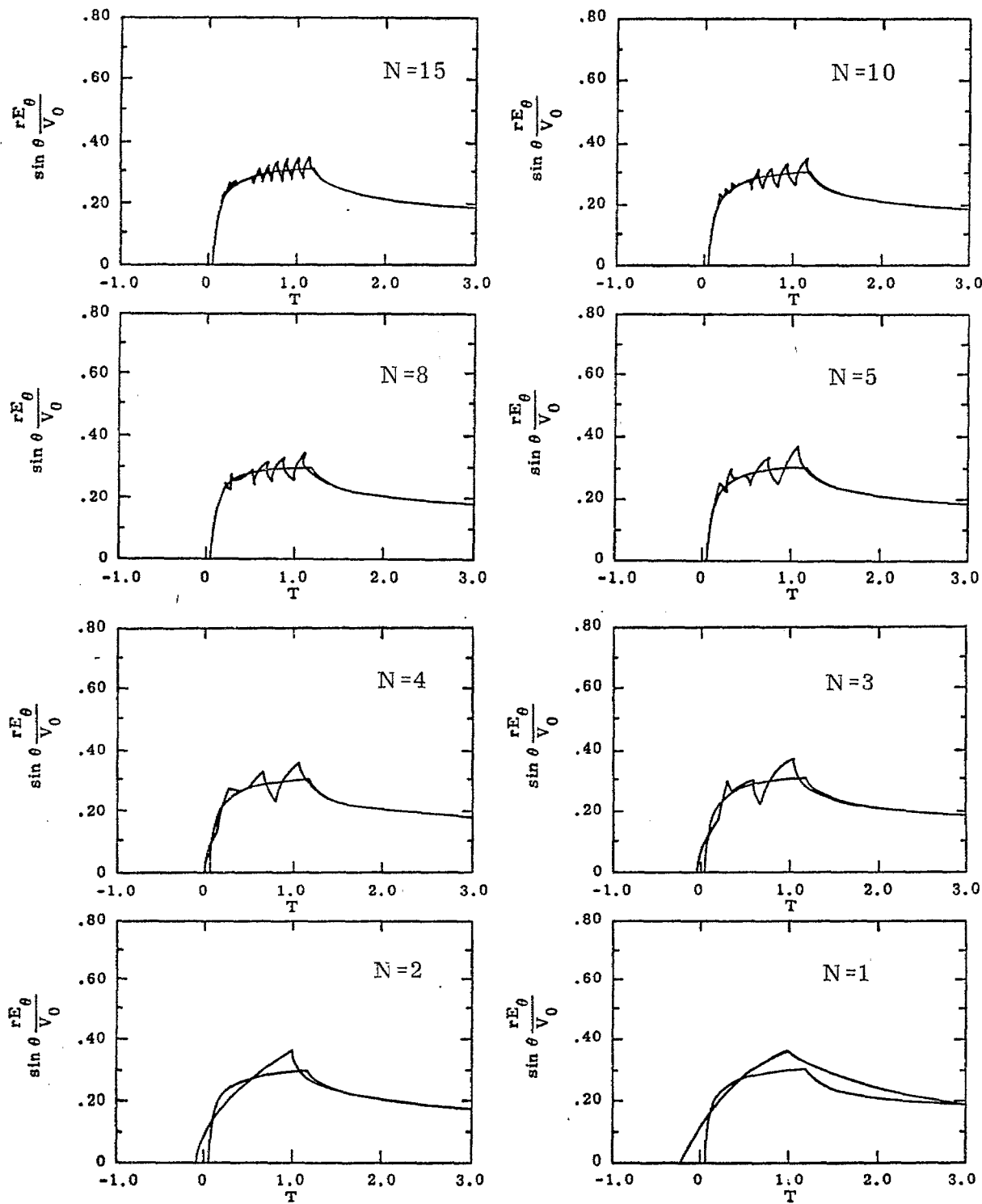


Figure 21. Radiation Field for bicone angle of $\theta_b = .6 \pi/2$ observed at $\theta_o = .4 \pi/2$ for various values of source gaps, N .

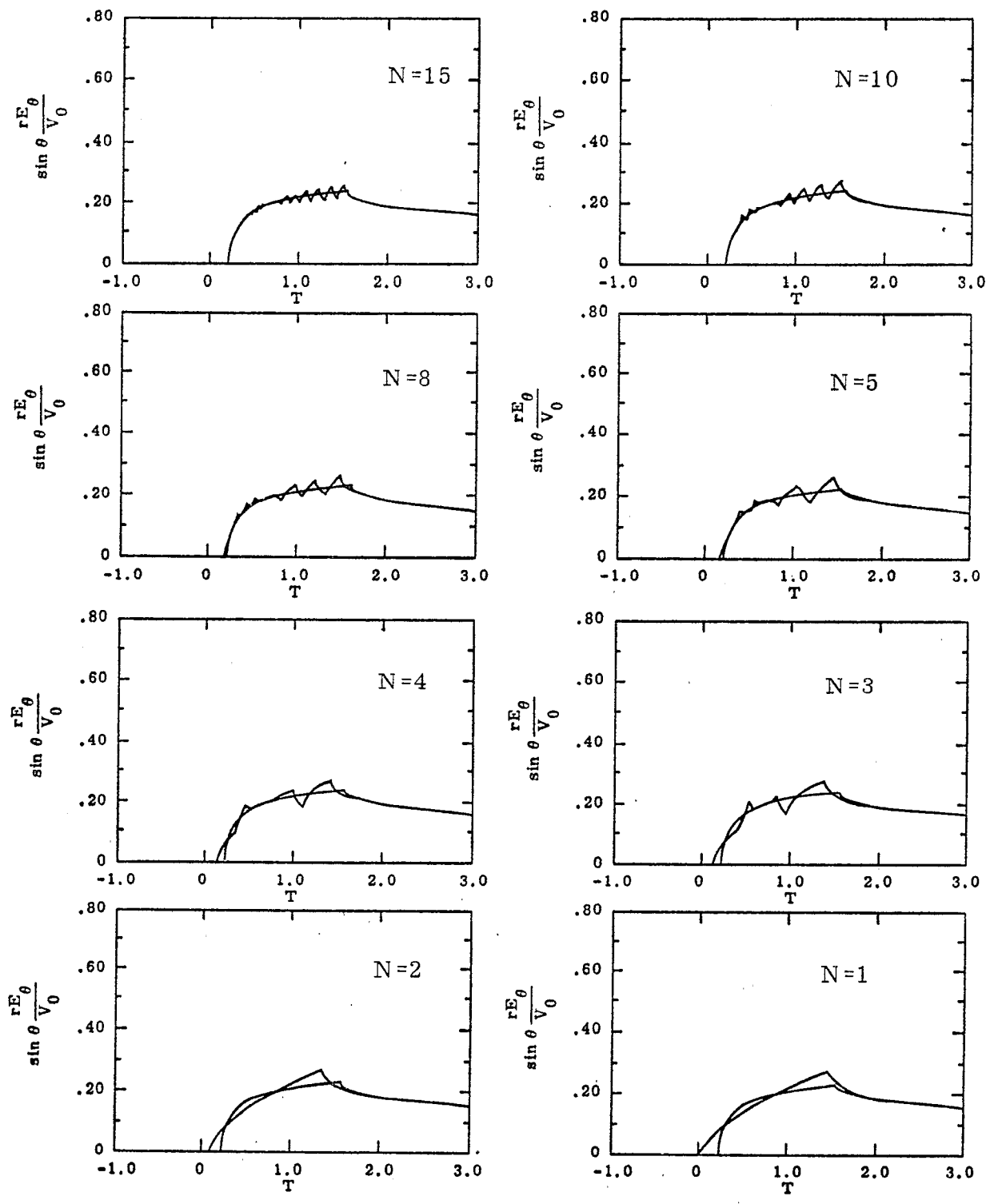


Figure 22. Radiation Field for bicone angle of $\theta_b = .6 \pi/2$ observed at $\theta_o = .2 \pi/2$ for various values of source gaps, N .

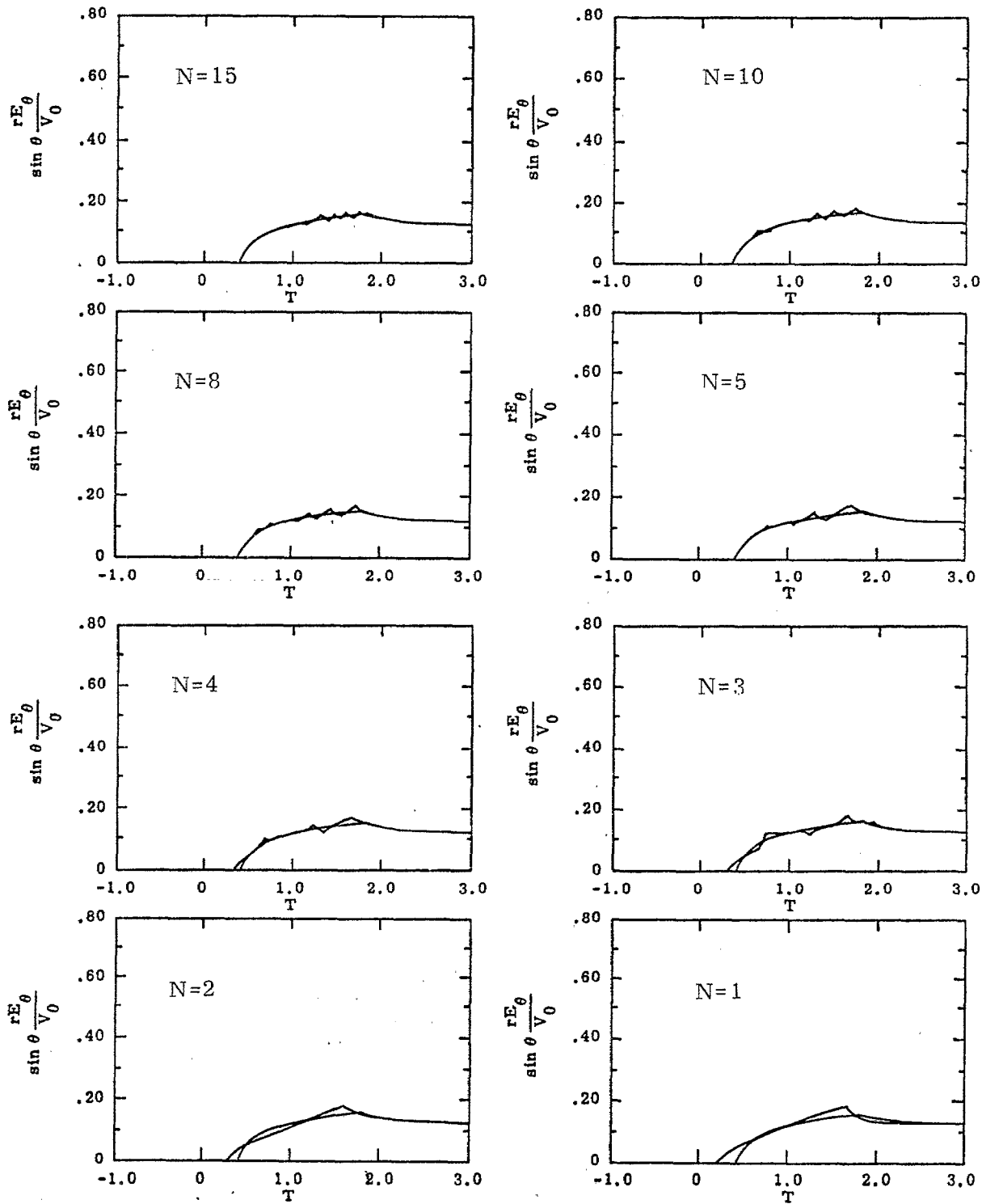


Figure 23. Radiation Field for bicone angle of $\theta_b = .6 \pi / 2$ observed at $\theta_o = .05 \pi / 2$ for various values of source gaps, N .

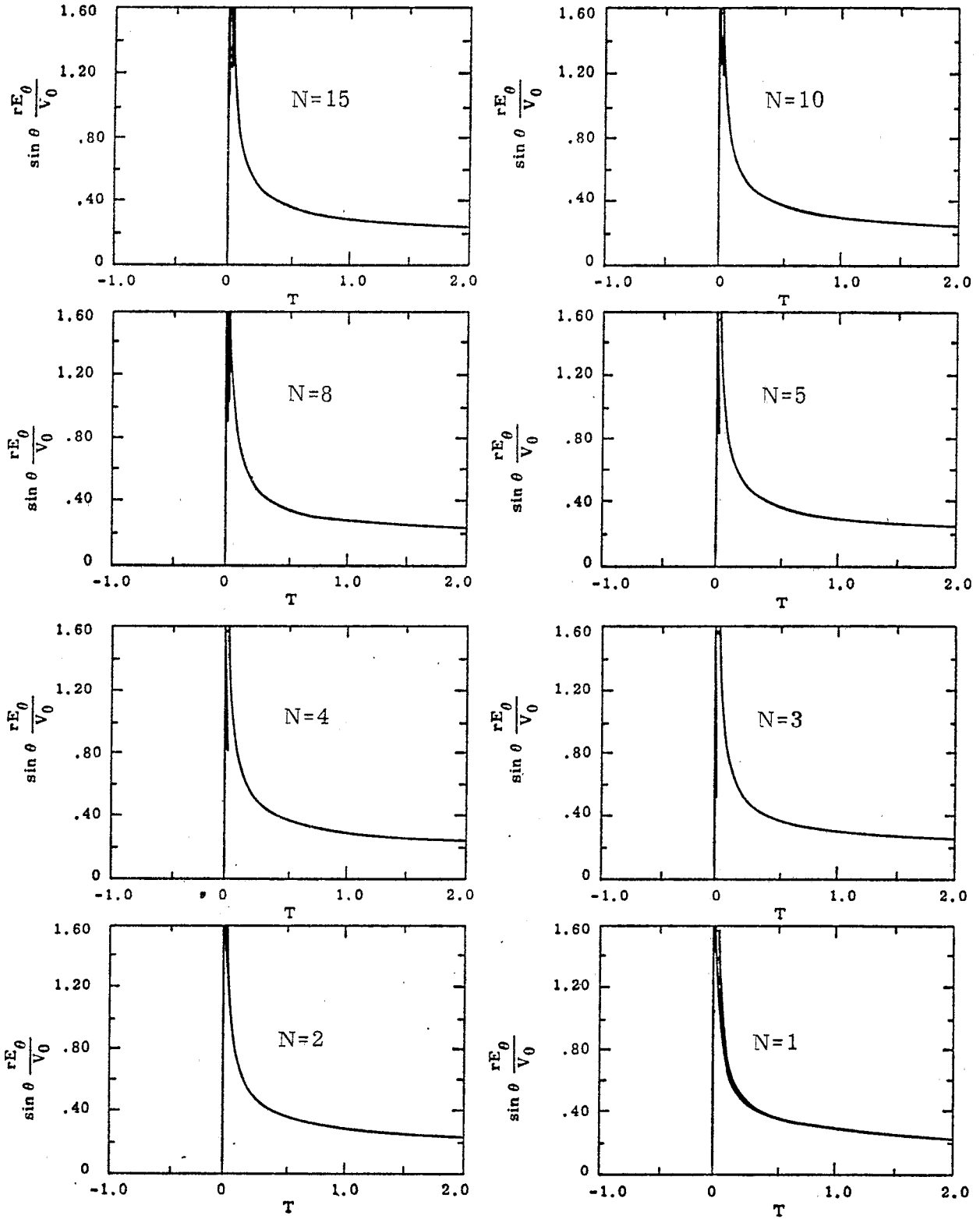


Figure 24. Radiation Field for bicone angle of $\theta_b = .8 \pi / 2$ observed at $\theta_o = 1.0 \pi / 2$ for various values of source gaps, N .

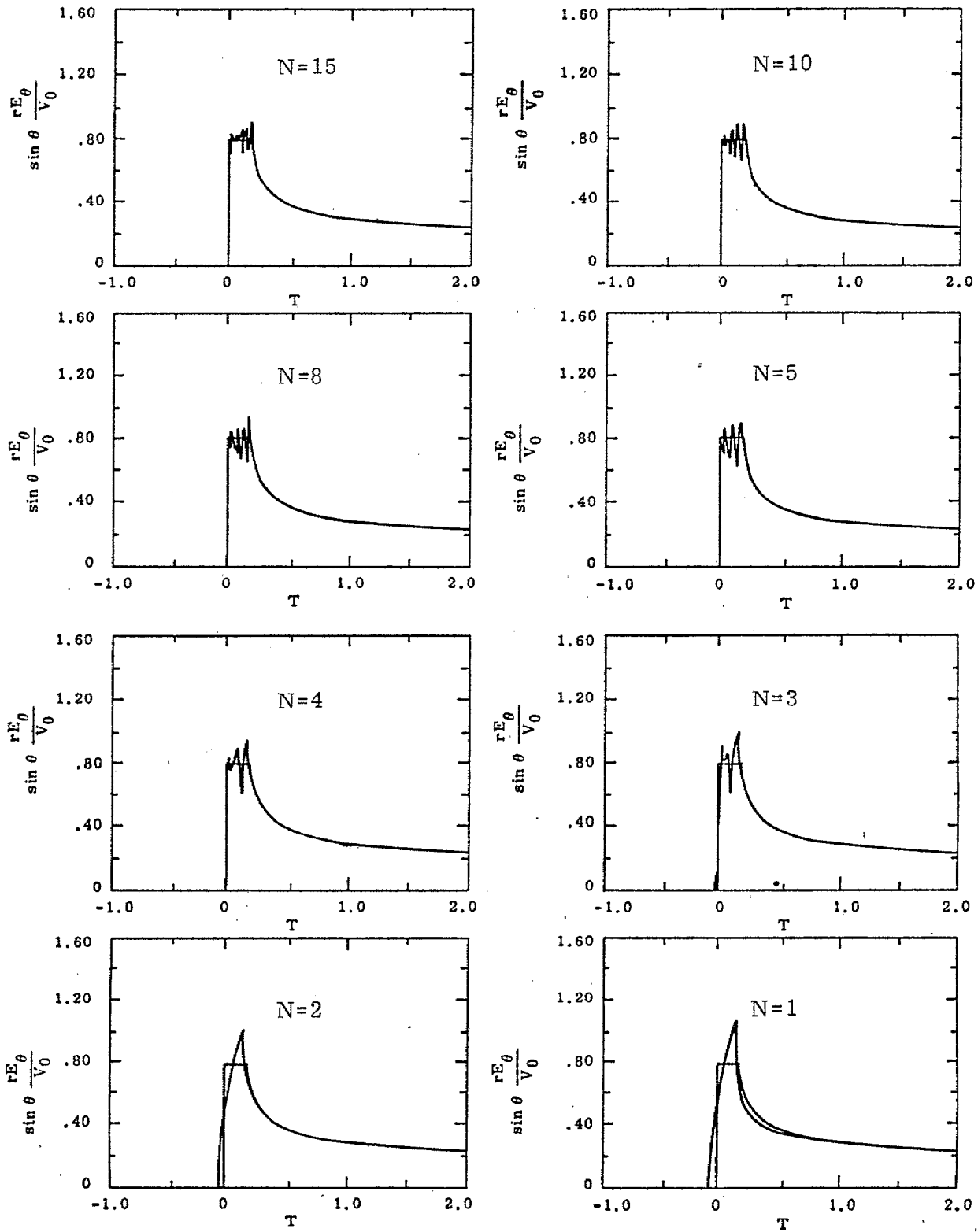


Figure 25. Radiation Field for bicone angle of $\theta_b = .8 \pi / 2$ observed at $\theta_o = .8 \pi / 2$ for various values of source gaps, N .

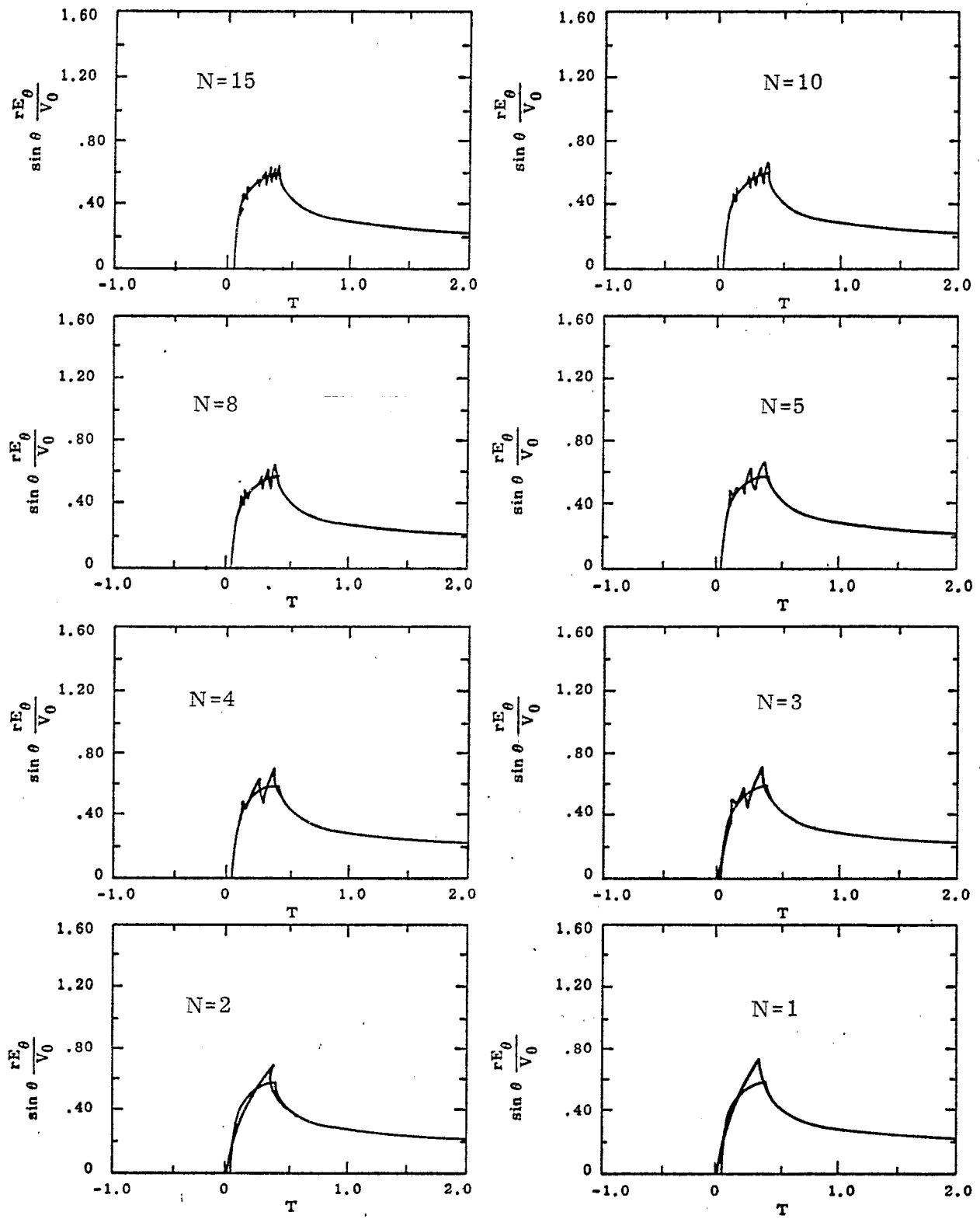


Figure 26. Radiation Field for bicone angle of $\theta_b = .8 \pi / 2$ observed at $\theta_o = .6 \pi / 2$ for various values of source gaps, N .

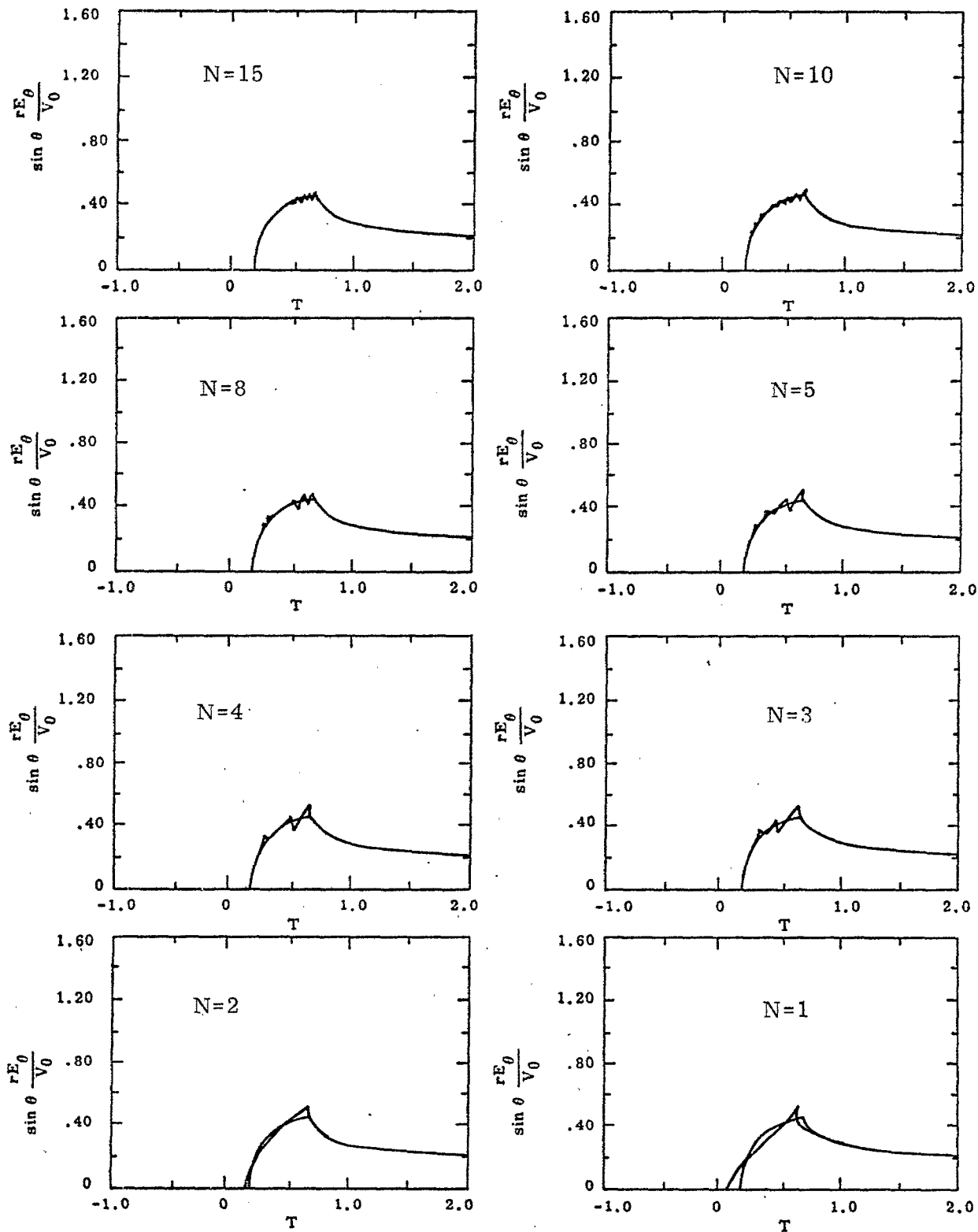


Figure 27. Radiation Field for bicone angle of $\theta_b = .8 \pi / 2$ observed at $\theta_o = .4 \pi / 2$ for various values of source gaps, N.

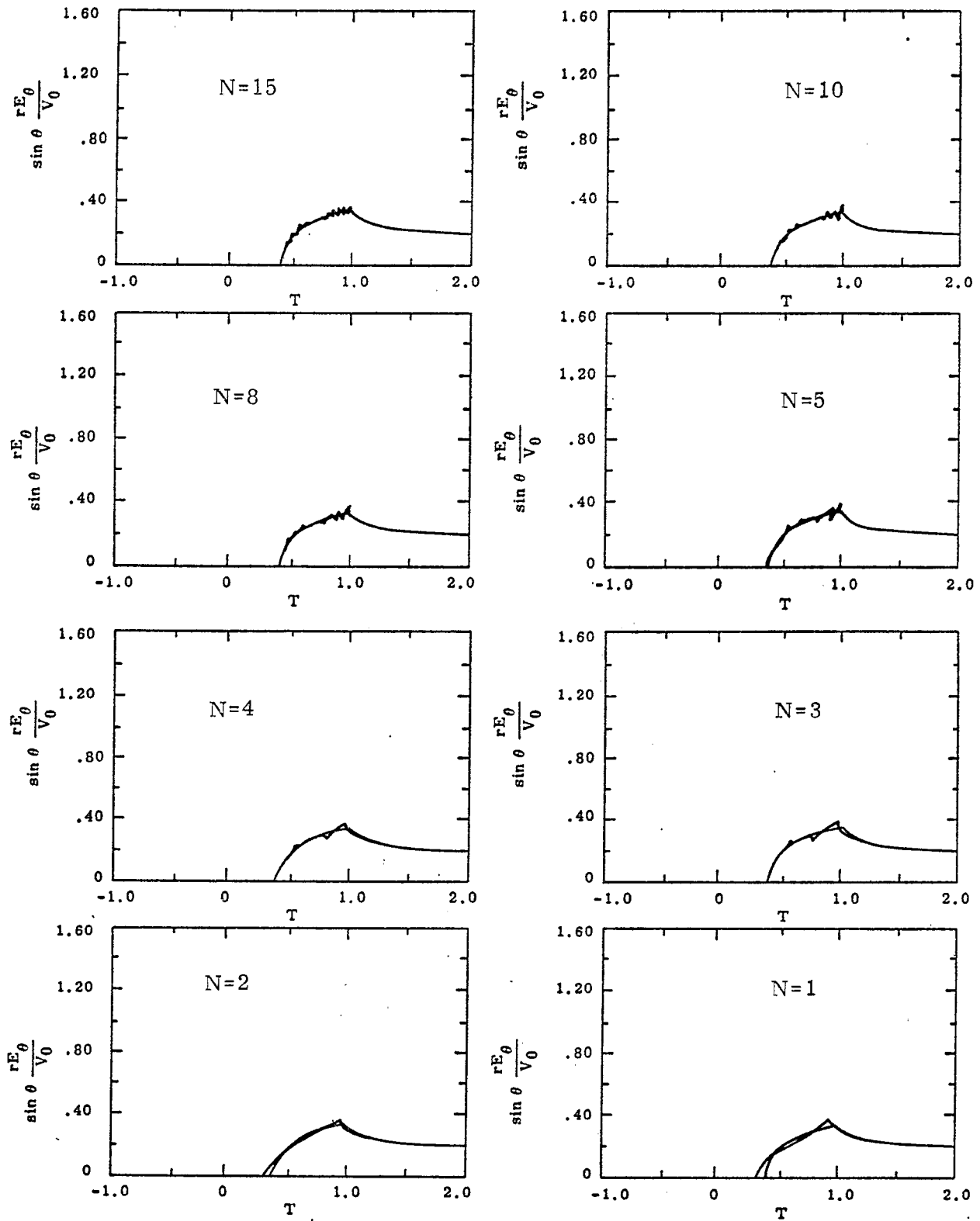


Figure 28. Radiation Field for bicone angle of $\theta_b = .8 \pi / 2$ observed at $\theta_o = .2 \pi / 2$ for various values of source gaps, N .

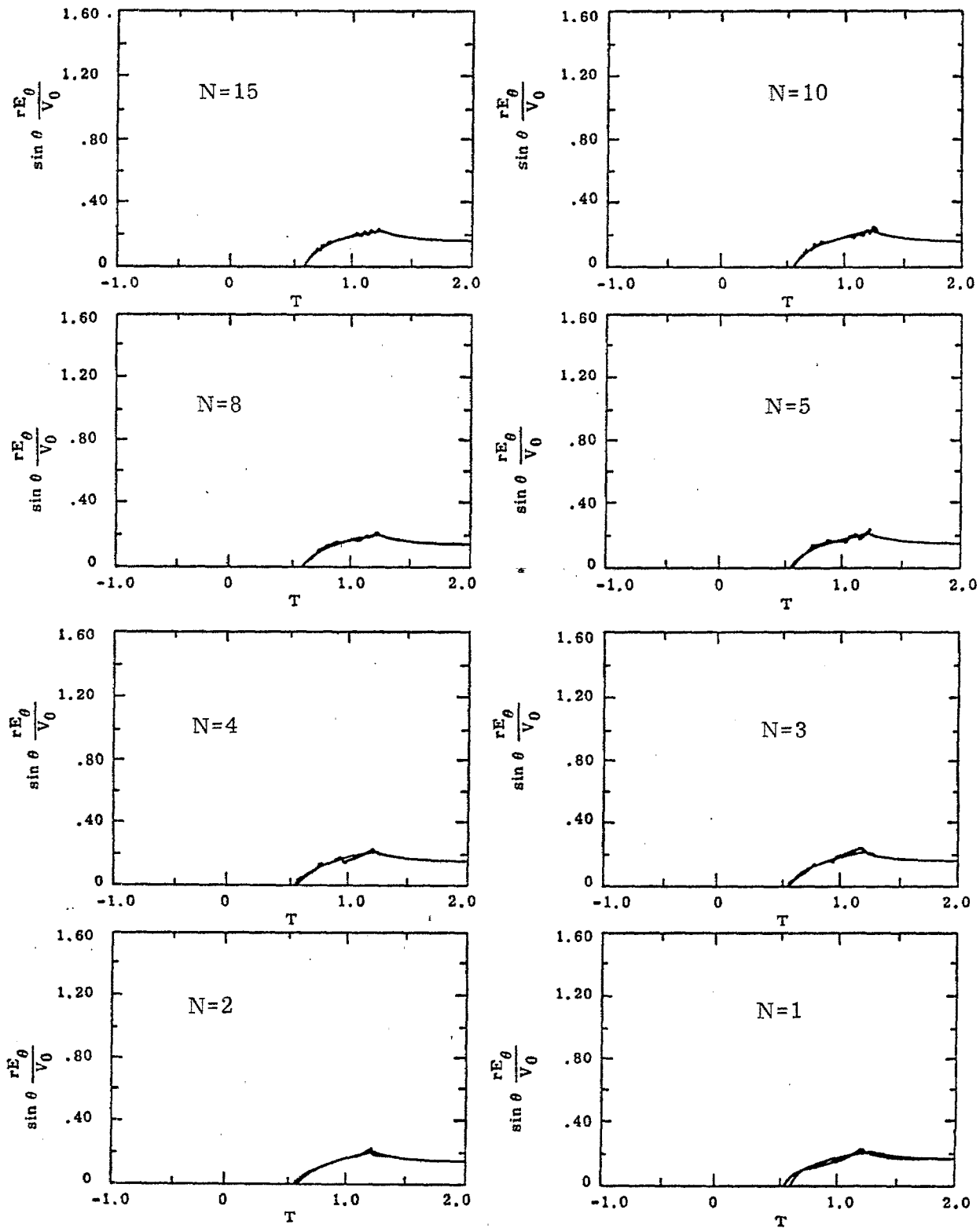


Figure 29. Radiation Field for bicone angle of $\theta_b = .8 \pi / 2$ observed at $\theta_o = .05 \pi / 2$ for various values of source gaps, N .

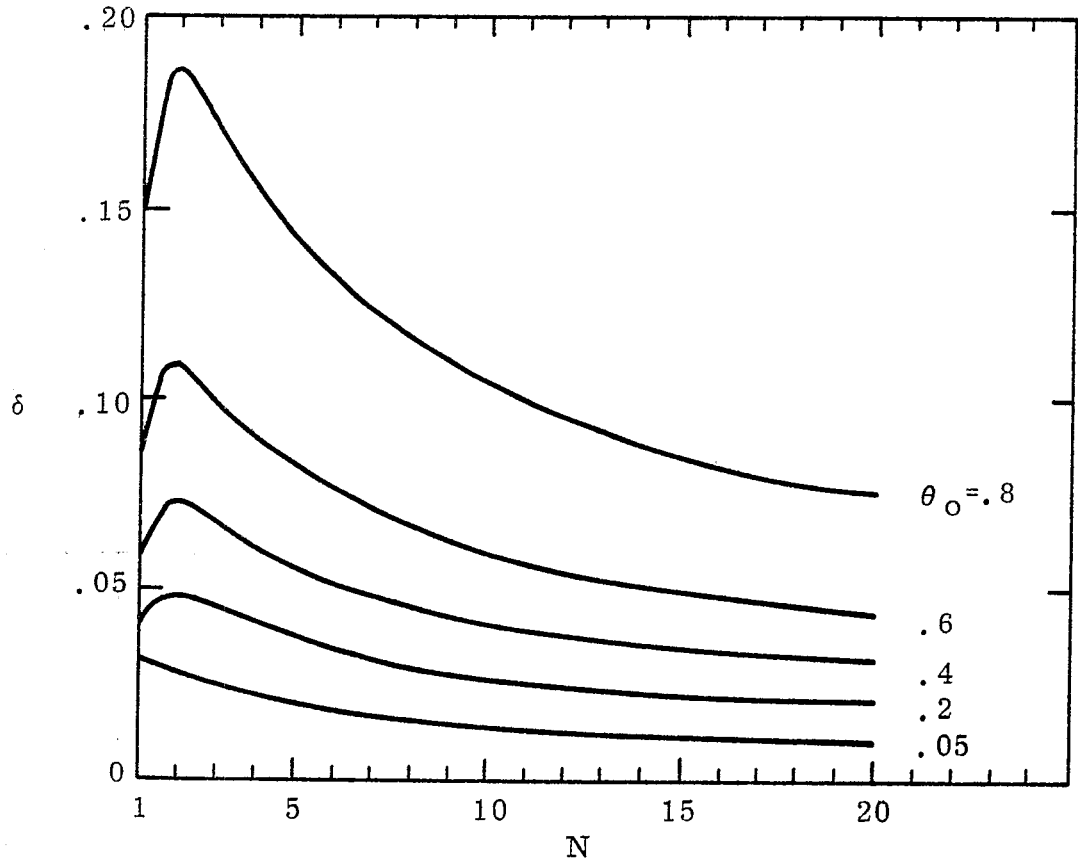


Figure 30. Plots of the maximum overshoot of the radiated field compared with the biconical field for $\theta_b = .2 \pi/2$, as a function of the number of discrete sources, N.

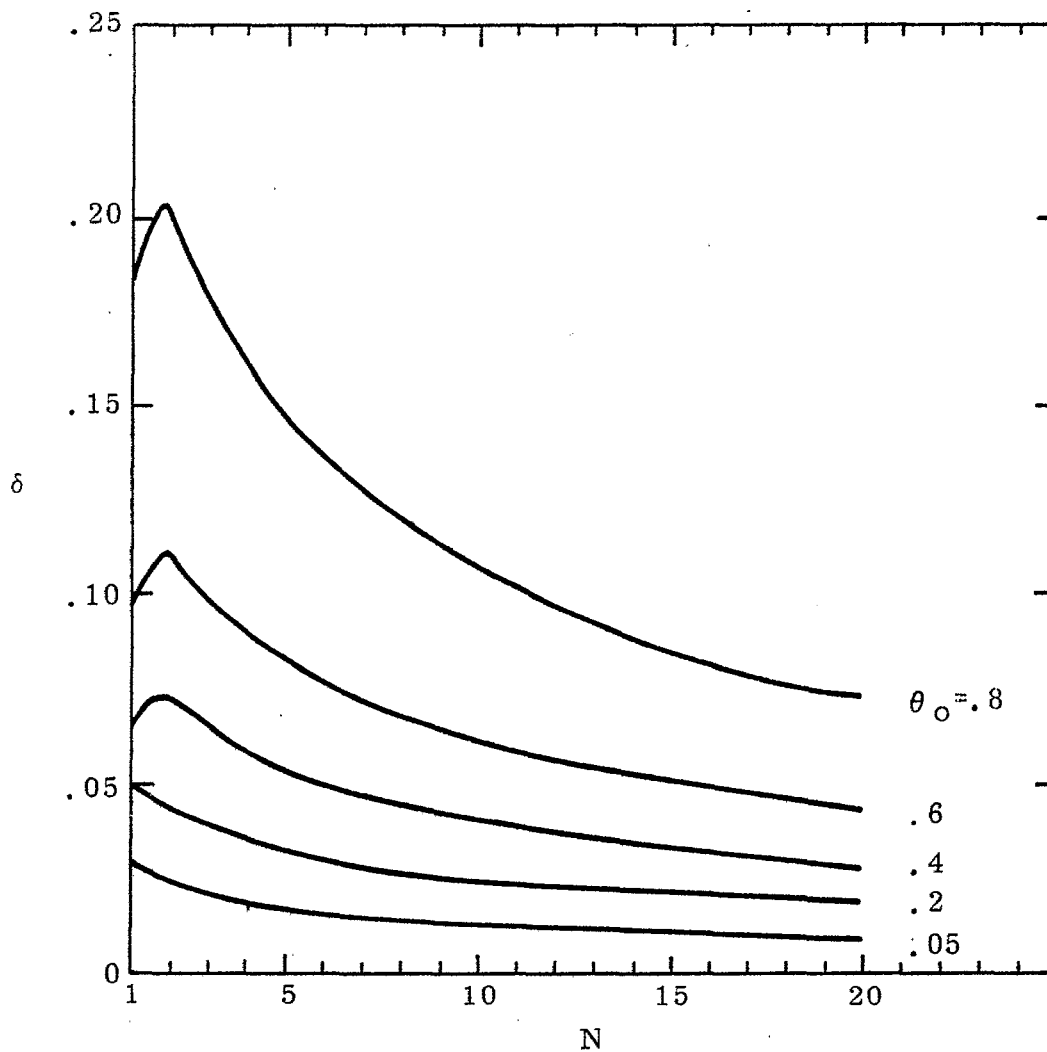


Figure 31. Plots of the maximum overshoot of the radiated field compared with the biconical field for $\theta_b = .8 \pi/2$, as a function of the number of discrete sources, N .

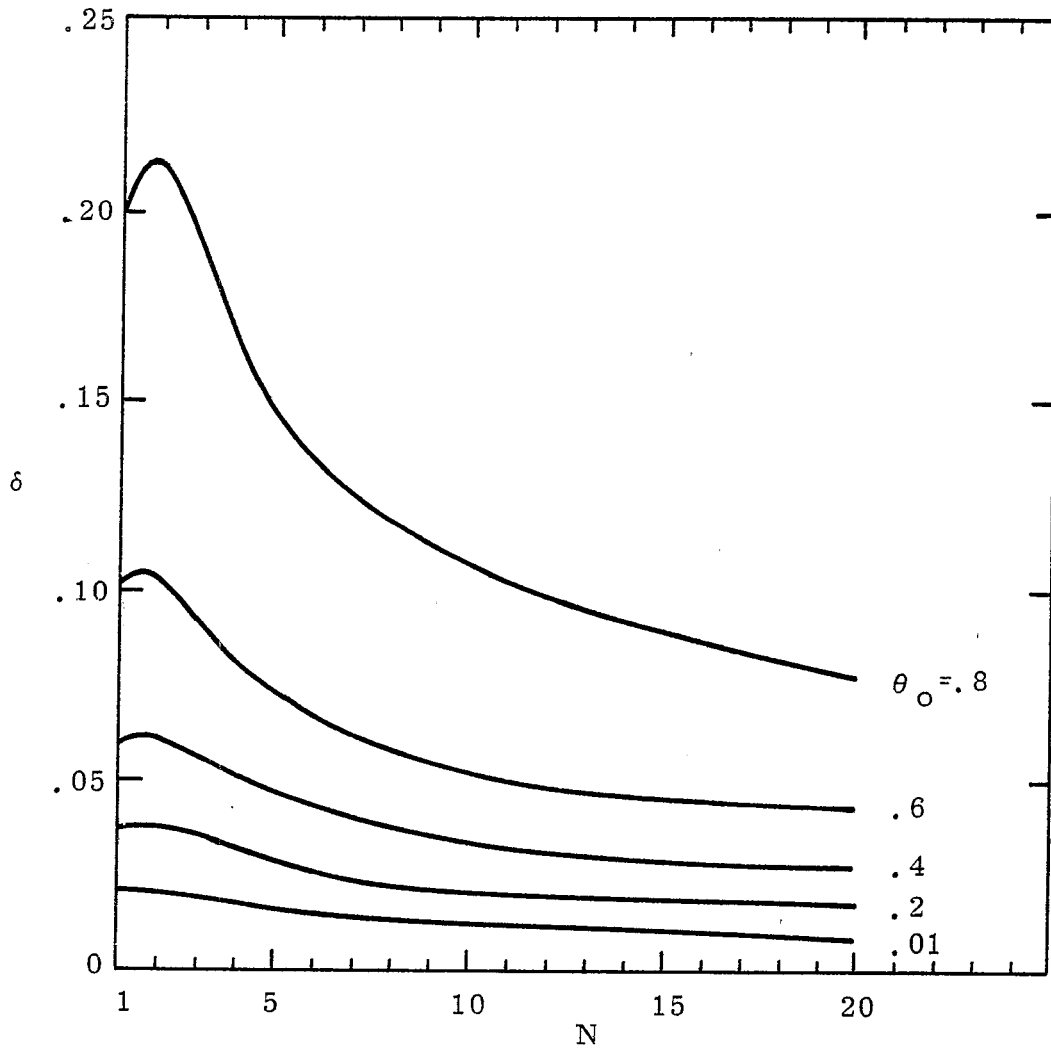


Figure 32. Plots of the maximum overshoot of the radiated field compared with the biconical field for $\theta_b = .6 \pi/2$, as a function of the number of discrete sources, N .

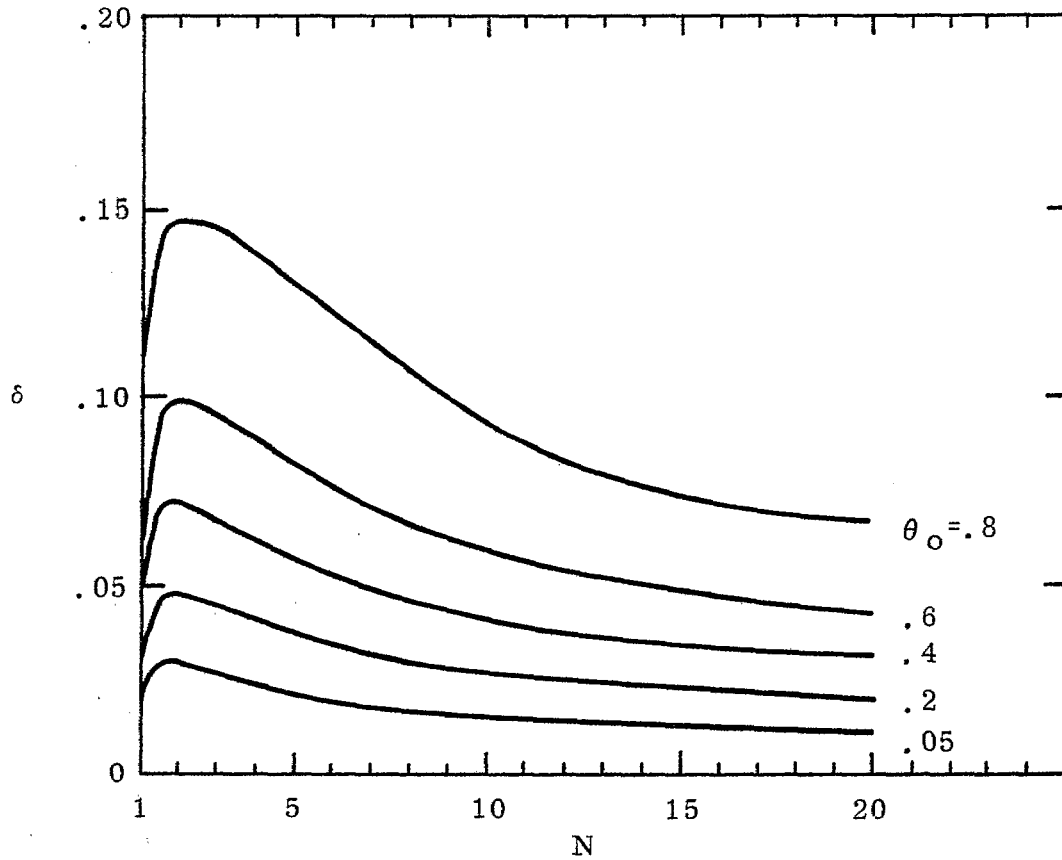


Figure 33. Plots of the maximum overshoot of the radiated field compared with the biconical field for $\theta_b = .4 \pi/2$, as a function of the number of discrete sources, N.

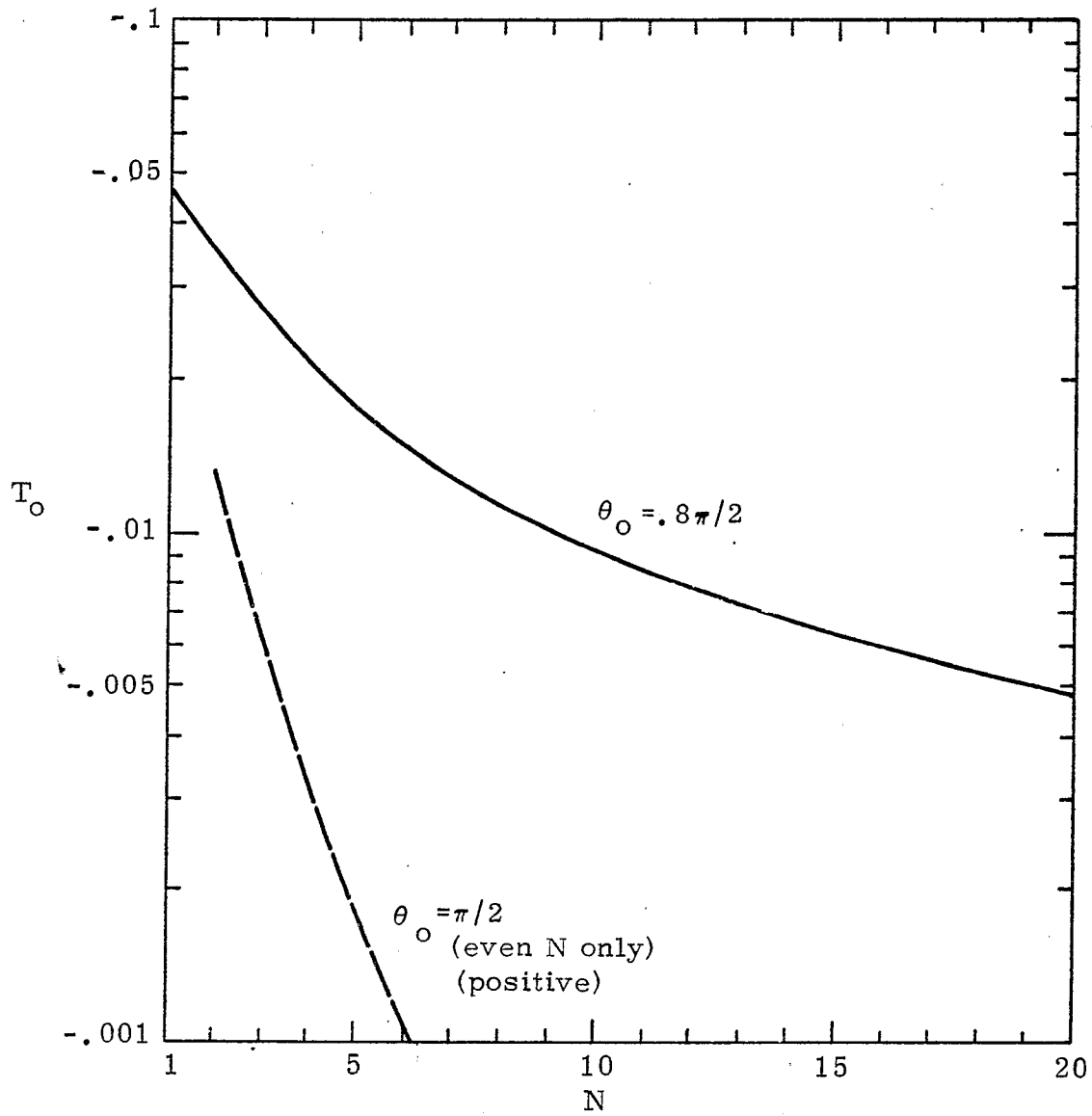


Figure 34. Plot of the turn-on time T_o for bicone angle $\theta_b = .8\pi/2$ (illuminated region only), as a function of N .

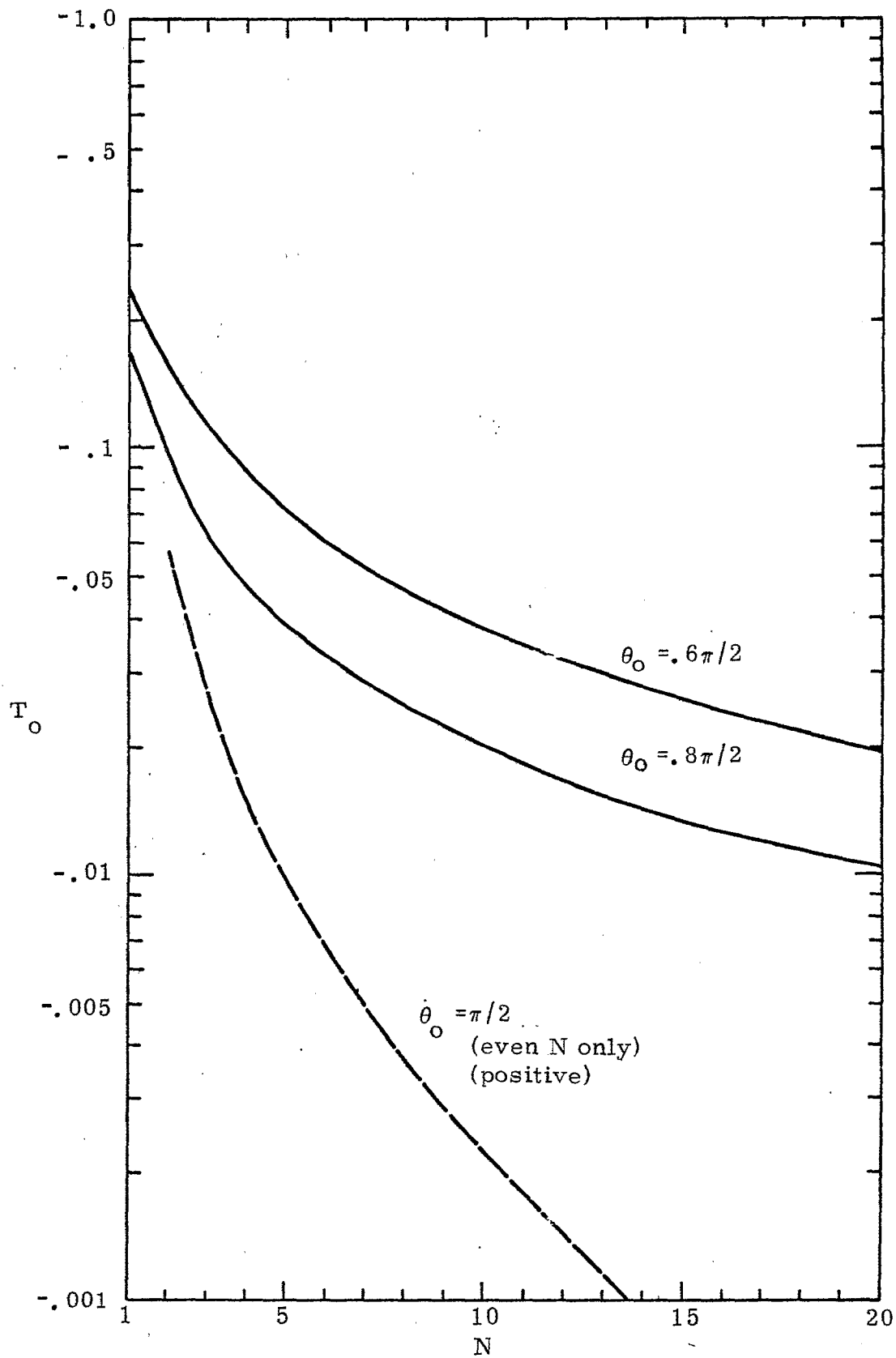


Figure 35. Plot of the turn-on time T_0 for bicone angle $\theta_b = .6\pi/2$ (illuminated region only), as a function of N .

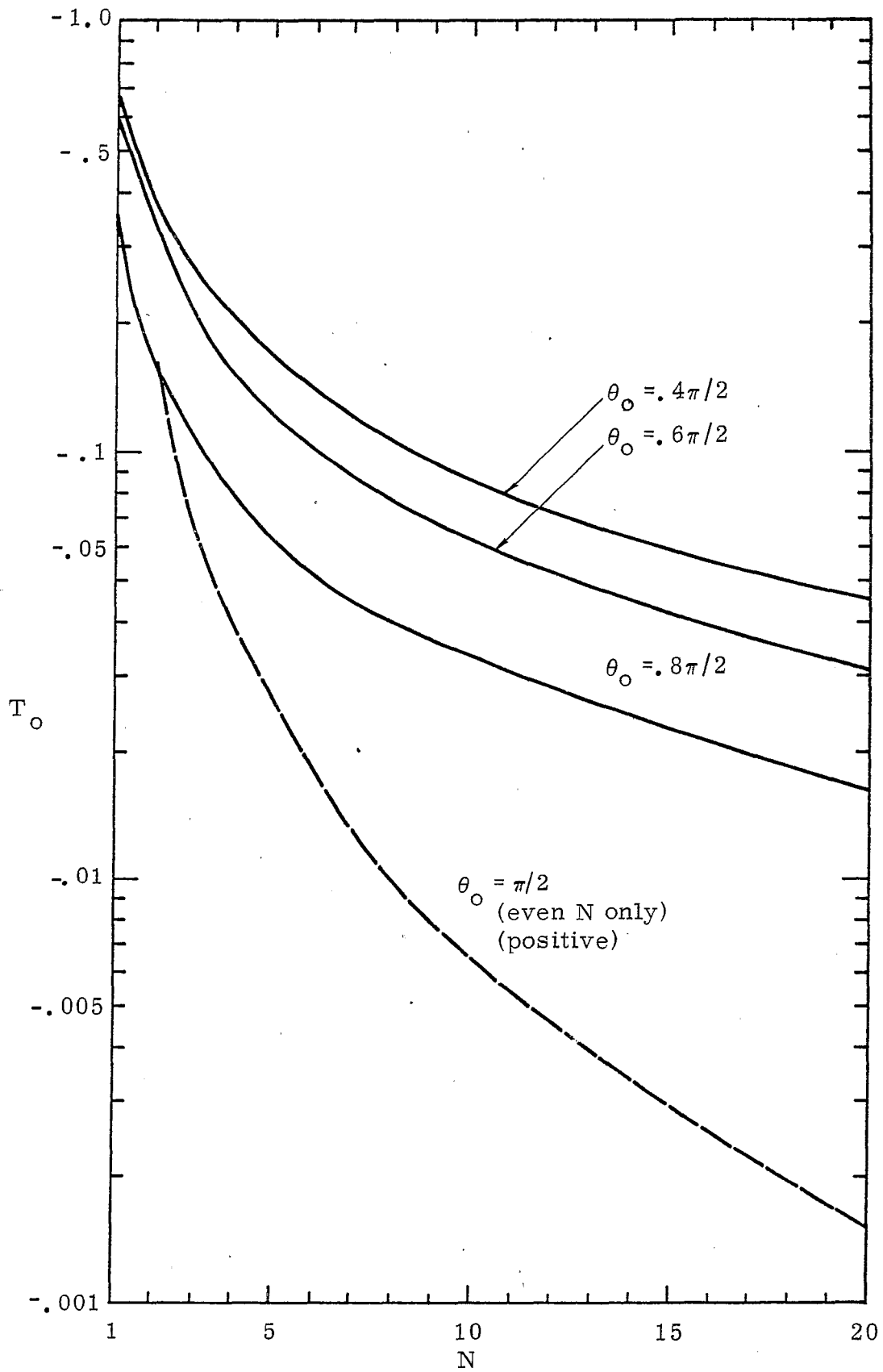


Figure 36. Plot of the turn-on time T_0 for bicone angle $\theta_b = .4\pi/2$ (illuminated region only), as a function of N .

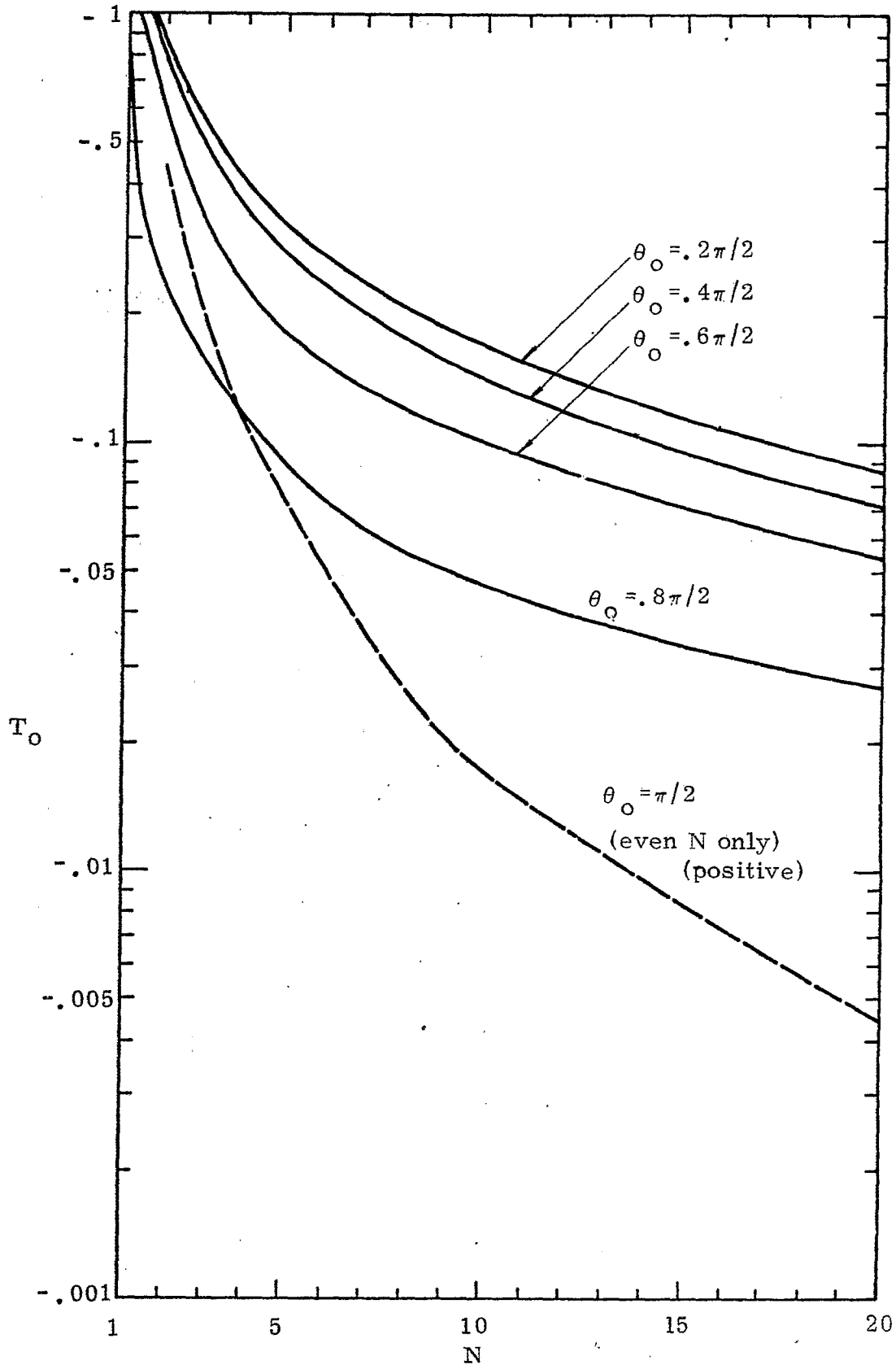


Figure 37. Plot of the turn-on time T_0 for bicone angle $\theta_b = .2\pi/2$ (illuminated region only), as a function of N .

V. References

1. Barnes, Paul R., "Pulse Radiation by an Infinitely Long, Perfectly Conducting, Cylindrical Antenna in Free Space Excited by a Finite Cylindrical Distributed Source Specified by the Tangential Electric Field Associated with a Biconical Antenna," Sensor and Simulation Note 110, July 1970.
2. Baum, Carl E., "Design of a Pulse-Radiating Dipole Antenna as Related to High-Frequency and Low-Frequency Limits," Sensor and Simulation Note 69, 13 January 1969.
3. Baum, Carl E., "The Distributed Source for Launching Spherical Waves," Sensor and Simulation Note 84, May 1969.
4. Latham, R. W., and K.S.H. Lee, "Pulse Radiation and Synthesis by an Infinite Cylindrical Antenna," Sensor and Simulation Note 73, February 1969.
5. Latham, R. W., and K.S.H. Lee, "Waveforms near a Cylindrical Antenna," Sensor and Simulation Note 89, June 1969.
6. Latham, R. W., and K.S.H. Lee, "Transient Properties of an Infinite Cylindrical Antenna," Radio Science, Vol. 5, No. 4, April 1970, pp. 715, 723.
7. Papas, C. H., "On the Infinitely Long Cylindrical Antenna," J. Appl. Phys., Vol. 20, No. 5, 1948, pp. 437-440.
8. Pine, Zoe Lynda, and F. M. Tesche, "Pulse Radiation by an Infinite Cylindrical Antenna with a Source Gap with a Uniform Field," Sensor and Simulation Note 159, October 1972.